UTTAC-83, 2014

UTTAC

ANNUAL REPORT 2013

TANDEM ACCELERATOR COMPLEX
Research Facility Center for Science and Technology
University of Tsukuba

http://www.tac.tsukuba.ac.jp/

UTTAC

ANNUAL REPORT 2013

April 1, 2013 – March 31, 2014

UTTAC-83, 2014

Executive Editor: Eiji Kita
Editors: Hiromi Kimura, Tetsuaki Moriguchi, Daiichiro Sekiba and Kimikazu Sasa

---

UTTAC is a series of issues, which include annual reports of
Tandem Accelerator Complex, Research Facility Center
for Science and Technology, University of Tsukuba.

Tandem Accelerator Complex, Research Facility Center for Science and Technology,
University of Tsukuba
Tennodai 1-1-1, Tsukuba, Ibaraki 305-8577, Japan

http://www.tac.tsukuba.ac.jp/
annual@tac.tsukuba.ac.jp

PREFACE

This annual report covers research conducted at the Tandem Accelerator Complex, Research Facility Center for Science and Technology, the University of Tsukuba, during fiscal year 2013 (April 1, 2013–March 31, 2014). After the Great East Japan Earthquake on March 11, 2011, research has been limited to that using the 1 MV Tandetron accelerator and radiation source experiments, ^{57}Fe Mössbauer spectroscopy, and positron annihilation spectroscopy. The circumstances of our research have not changed much and are almost the same as those in the last fiscal year. Thus, this volume has slightly fewer pages than older volumes like one for the last year.

A new 6 MV tandem-type accelerator with support from the government has reached at mid of March 2014 from the National Electrostatics Corporation in Middleton, Wisconsin, USA to the TAC. We are hoping to restart our research activities again after the installation.

The efforts of Open Advanced Facilities Initiative supported by MEXT were continued in this term, and the second stage was completed. The government supported additional facilities related to this program with an extra budget. With this support, our performance on this program is accelerated.

We are really looking forward to operating and reporting on the new 6 MV accelerator.

Editors

CONTENTS

1.

ACCELERATOR AND FACILITIES

1.1 Accelerator operation 2013

K. Sasa, S. Ishii, H. Kimura, H. Oshima, Y. Tajima, T. Takahashi, Y. Yamato,
T. Komatsubara, D. Sekiba and E. Kita

We have operated and maintained the 1 MV Tandetron accelerator and the radio-isotope utilization equipment in the University of Tsukuba, Tandem Accelerator Complex (UTTAC). In addition, we have constructed the 6 MV tandem accelerator instead of the broken 12UD Pelletron tandem accelerator.

The total service time of the UTTAC multi-tandem accelerator facility was 2,064 hours in the fiscal year 2013. The number of facility users is 106 on campus and 12 outside the campus. 648 hours for the 1 MV Tandetron accelerator and 14 days for the radio-isotope utilization equipment were used for industrial users under the project "Promotion of Advanced R&D Facility Utilization", which was supported financially by the Ministry of Education, Culture, Sports, Science and Technology (MEXT) of JAPAN. In the project, a total of 12 research programs were conducted in 2013.

The 1 MV Tandetron accelerator

The operating time and the experimental beam time of the 1 MV Tandetron accelerator were 1357.1 and 798 hours, respectively, during the total service time in 2013. A total of 66 research programs were carried out and a total of 725 researchers used the 1 MV Tandetron accelerator. Figure 1 shows the percentage of accelerated ions for the 1 MV Tandetron accelerator. In 2013, H beams accounted for 79.2 % of ion acceleration. O beams were mainly used for high-resolution ERDA. Figure 2 shows the percentage of research fields for the 1 MV Tandetron accelerator in 2013.

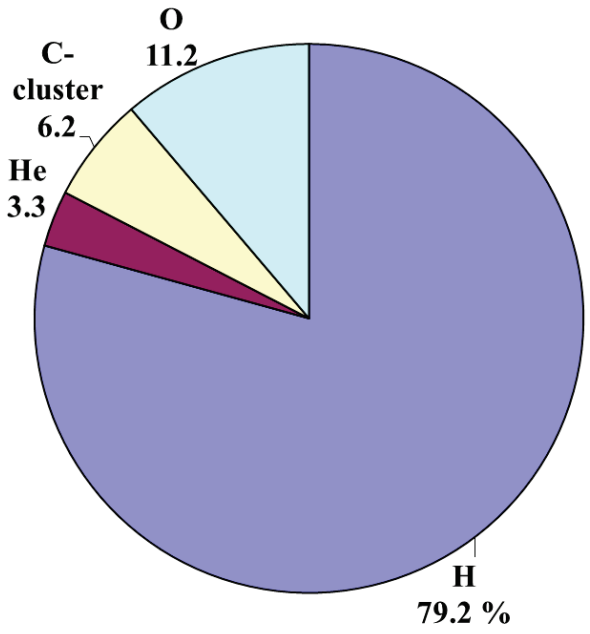

Figure 1. Percentage of accelerated ion species for the 1 MV Tandetron accelerator in 2013.

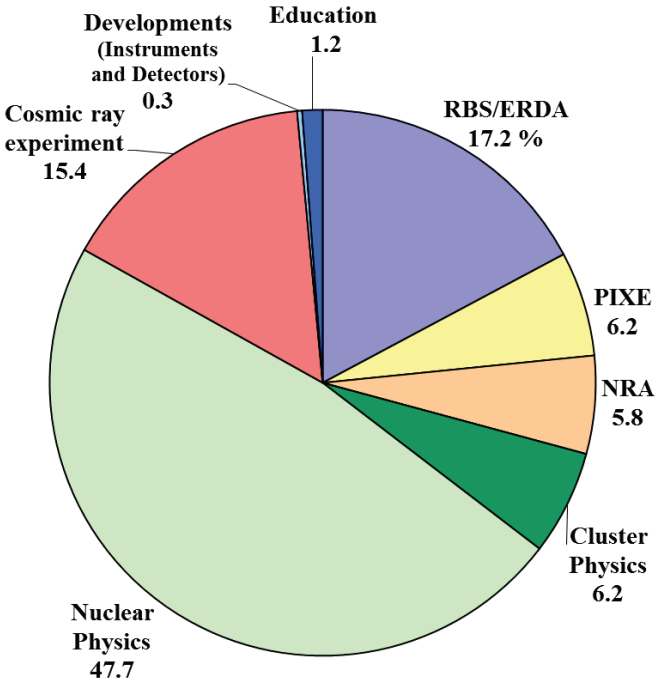

Figure 2. Percentage of research fields for the 1 MV Tandetron accelerator in 2013.

1.2 Installation of the 6 MV tandem accelerator

K. Sasa, S. Ishii, H. Kimura, H. Oshima, Y. Tajima, T. Takahashi, Y. Yamato,
T. Komatsubara, D. Sekiba and E. Kita

A new tandem accelerator system has been designed and constructed at the University of Tsukuba after the Great East Japan Earthquake [1, 2]. The accelerator system consists of the 6 MV Pelletron tandem accelerator, four negative ion sources, a Lam-shift polarized ion source (PIS), a vertical irradiation line and 12 beam lines. A high energy beam transport line connects from the accelerator room to present experimental facilities at the experimental room. The 6 MV Pelletron tandem accelerator will be applied to multi-purpose ion beam researches such as AMS, microbeam applications, PIXE analysis for geoscience and material research, heavy ion RBS/ERDA, nuclear reaction analysis (NRA) for hydrogen in material, high energy ion irradiation for semiconductor and nuclear physics. Figure 1 shows a most recent layout of the 6 MV tandem accelerator system in the accelerator room.

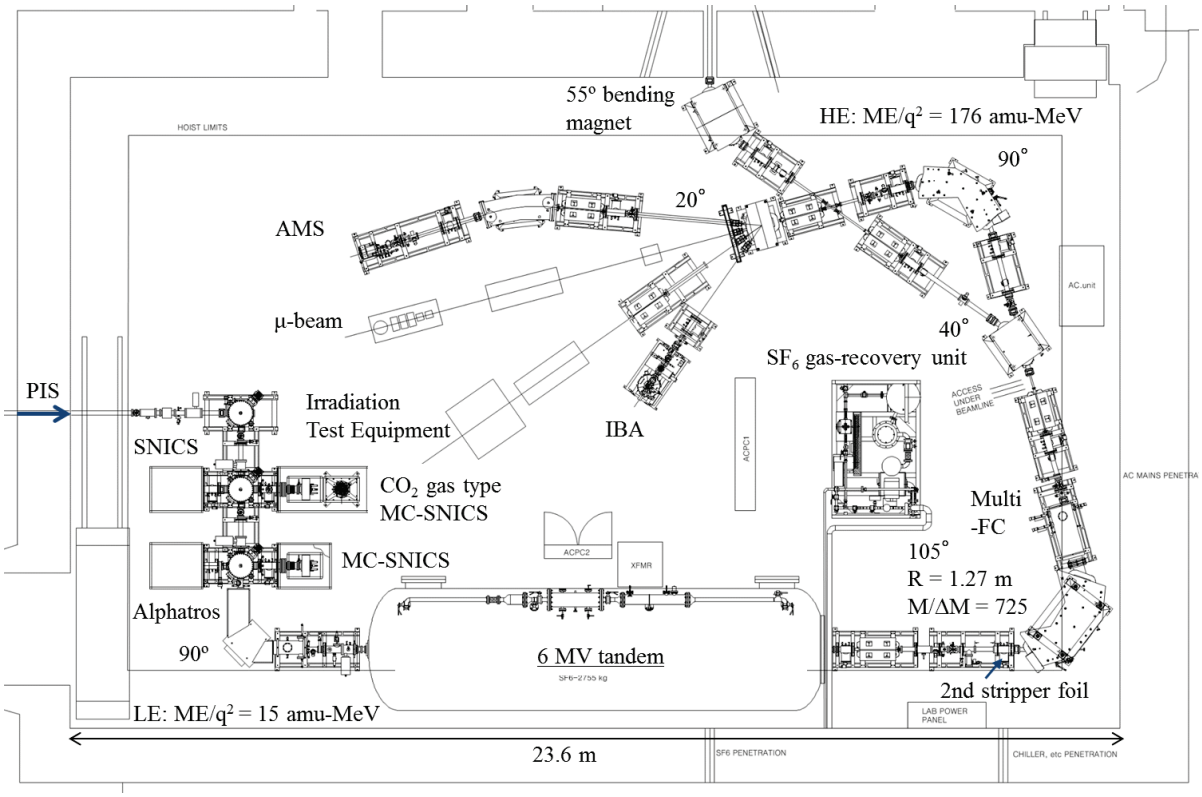

Figure 1. Layout of the 6 MV tandem accelerator system in the accelerator room.

A high voltage test was already tried with a great deal of success at the National Electrostatics Corp. (NEC), USA in January, 2014. The generator was operated up to the maximum terminal voltages as high as 6.3 MV. A stability is estimated to be better than 1 kV at 6.0 MV terminal voltage. Maximum beam currents are estimated up to 50 μA for heavy ions. Figure 1 shows a photograph of setup for the high-voltage test at NEC.

Figure 1. Photograph of setup for the high-voltage test at NEC, USA in January, 2014.

The main accelerator, the model 18SDH-2 Pelletron accelerator developed by NEC, USA was installed at the University of Tsukuba on 6 March, 2014 (Figures 2 and 3). The accelerator tank was designed as about 2.74 m in diameter and 10.5 m in length. The high voltage terminal has a longer gas stripper tube assembly and a foil changer with 80 foil holders for electron stripping of negative ions. At present, we have constructed ion sources and beam lines. The accelerator operation will start at the fiscal year 2015.

Figure 2. The accelerator tank was delivered to Tsukuba on 6 March 2014.

Figure 3. Setup of the accelerator tank in the accelerator room

References

[1] Kimikazu Sasa et al., AIP Conf. Proc. 1533, pp. 184-188; doi: http://dx.doi.org/10.1063/1.4806798.

[2] Kimikazu Sasa et al., UTTAC, ANNUAL REPORT 2012, UTTAC-82, 2013, 3.

2.

NUCLEAR PHYSICS

2.1 Reaction cross section of ^{45}Sc(p, α)^{42}Ca for basis of silicon burning

T. Komatsubara[1], T. Onishi, M. Mukai, D. Izumi, Y. Saito, N. Inaba, K. Sawahata, T. Hayakawa[2], T. Shizuma[2], H. Yamaguchi[3], S. Kubono[4], D. Nagae, K. Sasa and A. Ozawa

Silicon burning is a sequence of reactions which create from silicon to iron at the final stage of the evolution of stars. When temperature of stars rise up to be 3 ~ 5 GT by gravitational compression, nuclei of silicon are starting to be decomposed by thermal photodisintegration and to be protons, neutrons, and α particles. The emitted α particles can fuse with the silicon or heavier nuclei and the continuous fusion chain reaction can reach to create the iron[1]. Among those of (α, γ) and (p, γ) reactions, the flow of reactions is predicted to be concentrated on ^{45}Sc, which are ^{42}Ca(α, p)^{45}Sc and ^{45}Sc(p, γ)^{46}Ti reactions[2]. Then we have chosen the reversed reaction of ^{45}Sc(p, α)^{42}Ca to evaluate the forward reaction rate, because experimental information of the lower energy part of the reaction cross sections was quite limited [3].

Experimental study was carried out by using the 1 MV Tandetron accelerator at UTTAC. Proton beam having the energy of 1.8 ~ 2.1 MeV was irradiated on the scandium target. The target was 40 μg/cm^2 in thickness made with evaporation of metallic scandium on a 53 μg/cm^2 carbon foil. Since Q-value of the ^{45}Sc(p, α)^{42}Ca reaction is rather large to be 2.34 MeV the emitted α particles can be determined with E-ΔE counter telescope consisted of two Si detectors. Thickness of the detectors are 10 μm for the ΔE counter and 1500 μm for the E counter, respectively. The thick E detector is necessary to have full stop proton peak. The detector was located at 49.5 mm (39.5 mm for the additional measurement) having the window of ϕ 7.0 mm diameter.

The measured angular distributions of the emitted α particle are shown in Fig. 1 for the proton beam energies of 1.8, 2.0, and 2.1 MeV. The distributions show rather flat, so that the distribution is assumed to be isotropic for other bombarding energies.

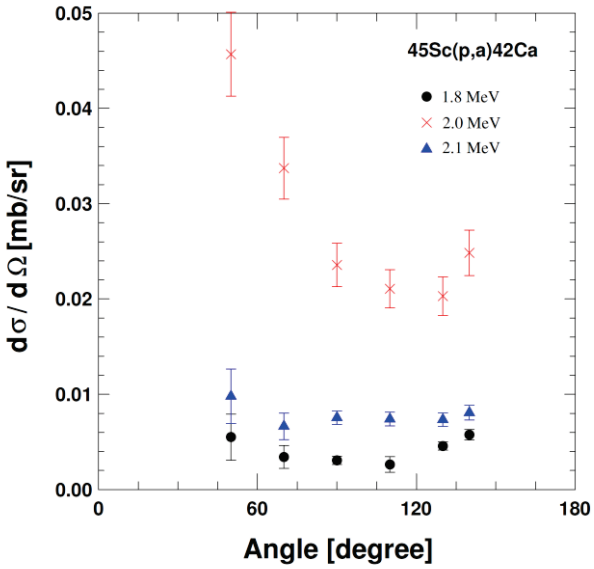

Fig. 1. Angular distribution of ^{45}Sc(p, α)^{42}Ca reaction.

Calculated astrophysical S-factor $S(E)$ from the measured cross sections for the ^{45}Sc(p, α)^{42}Ca reaction are shown in Fig. 2 comparing with the previous study by Schweitzer[3]. Reported data for the ^{42}Ca(α, p)^{45}Sc

[1] Present address: Institute for Basic Science, Yuseong-gu, Yuseong-daero, Daejeon, Republic of Korea
[2] Japan Atomic Energy Agency (JAEA), Tokai, Ibaraki, Japan
[3] Center for Nuclear Study, University of Tokyo, Hirosawa 2-1, Wako, Saitama, Japan
[4] RIKEN Nishina Center, Hirosawa 2-1, Wako, Saitama, Japan

reaction[4] are also consistent within the detailed balance[1] (not shown in this figure). A result of fitting with multilevel R-Matrix theory **SAMMY**[5] is also shown by the dashed lines. Parameters used for the fitting is tabulated in Table 1. With this fitting, the two peaks can be assigned as narrow resonances having spins of 1^- and 0^+ as shown in Fig. 2. In the previous report[6], a 0^+ state was reported at 12.46 MeV with ^{44}Ca(^{3}He, n)^{46}Ti reaction, which can be plausible state corresponding to our observed level at 12.31 MeV.

Since Gamow window can be estimated between 1.8 and 2.4 MeV for the silicon burning, the existence of the newly observed resonance at 2 MeV can significantly increase the reaction rate. Further continuous investigations are desirable to explore the astrophysical reaction rate for the silicon burning.

References

[1] C.E. Rolfs and W.S. Rodney, "Cauldrons in the Cosmos", The University of Chicago Press, 1988.

[2] S.E. Woosley *et al*., Astrophys J.S. **26** (1973) 231.

[3] J.S. Schweitzer *et al*., Nucl. Phys. **A287** (1977) 344.

[4] L.W. Mitchell *et al*., Nucl. Phys. **A443** (1985) 487.

[5] SAMMY-8, Radiation Safety Information Computational Center (RSICC), Oak Ridge National Laboratory.

[6] "Table of Isotopes, CD ROM Edition", R.B. Firestone and V.S. Shirley editor, (1996), LBL, Wiley-Interscience.

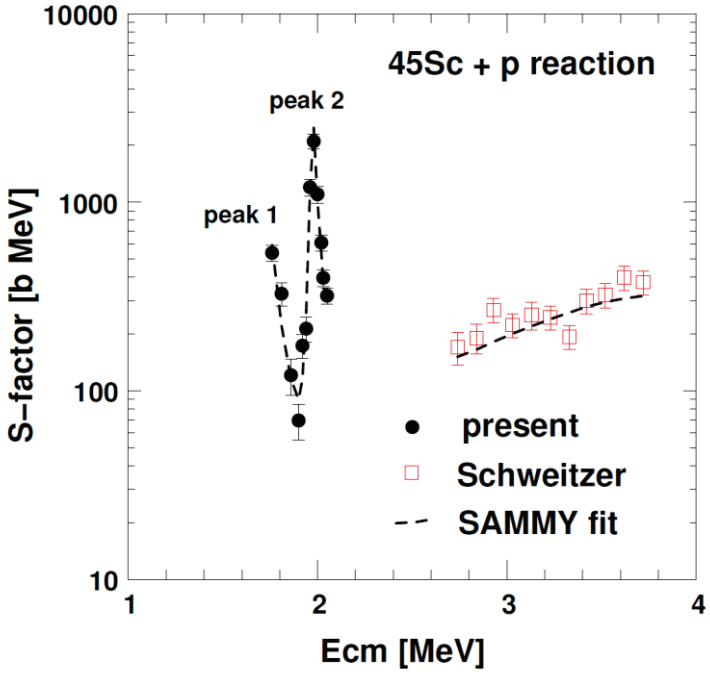

Fig. 2. Astrophysical S-factor for the ^{45}Sc(p, α)^{42}Ca reaction. Present results are shown by closed circles. Previous work done by Schweitzer[3] are shown by open squares. A result of SAMMY R-matrix fit[5] is shown by dashed lines.

Table 1. Parameters used for the SAMMY R-matrix fit[5] for the ^{45}Sc(p, α)^{42}Ca reaction as shown in the Fig. 2 with the dashed lines. In this fitting, two narrow resonances are obvious shown as peak1 and peak2 in the figure. The E_x denotes the excitation energy of compound nucleus ^{46}Ti. For the calculation of the energy E_x, a Q value of 10.345 MeV is used for the ^{45}Sc(p, γ)^{46}Ti reaction.

	E_{lab} [MeV]	E_{cm} [MeV]	J^{π}	Γ_p [keV]	Γ_α [keV]	Ex [MeV]
Peak 1	1.731	1.693	1^-	3.6 ± 0.7	1.5 ± 0.1	12.03
Peak 2	2.014	1.970	0^+	0.76 ± 0.02	29 ± 1	12.31

2.2 The experimental study of the astrophysical S-factor of ^{6}Li(p, γ)^{7}Be reaction

S.Z. Chen[1], J.J He[1], T. Komatsubara, S.B. Ma[1], S. Kubono[2], K. Sasa, A. Ozawa, A. Yamazaki, T. Onishi, M. Mukai, D. Izumi, H. Miyatake[3], D. Sekiba, T. Hayakawa[4], T. Shizuma[4], D. Kahl[5], C. Moon[6] and T. Kajino[7]

In the low-temperature astrophysics sites, e.g., our Sun, the Red Giant stars and the nova, the Gamow windows are well below the Coulomb barriers for the charged- particle-induced nuclear reactions involved. These nuclear reactions occur through the quantum-mechanics barrier penetration, sometimes referred to as the tunneling effect, with a small but finite probability. Because of the exponential behavior of the probability for tunneling, the reaction cross-section drops rapidly for energies below the Coulomb barrier. Frequently, the reaction cross-section is expressed as[1]:

$$\sigma = \frac{1}{E}\exp(-2\pi\eta)S(E) \tag{1}$$

The quantity η is called the Sommerfeld parameter and is defined as

$$\eta = \frac{Z_1 Z_2 e^2}{\hbar v} \tag{2}$$

In Eq. (1), the function $S(E)$, containing all the strictly nuclear effects, is referred to as the astrophysical S-factor [1]. In contrast to cross-section, the S-factor is a smoothly varying function of energy for the non-resonant reactions. With these characteristics, the factor $S(E)$ is much more useful in extrapolating measured cross-sections at higher energies to Gamow energies.

^{6}Li(p, γ)^{7}Be reaction and its reverse reaction are closely related to the big bang nucleosynthesis (BBN). It is worthwhile to determine the low-energy S-factors of ^{6}Li(p, γ)^{7}Be reaction. The measurement of this reaction has been done on 320 kV high voltage platform in Lanzhou and found an interesting sizable drop contrary to any existing theoretical expectations at energies below 200 keV [2]. Limited by the energy of 320 kV platform, we cannot cover the interesting energy region of 0.3~1 MeV to compare our data with previous results. It's necessary to investigate this reaction on a wider energy region accelerator.

A new measurement has been done on the 1 MeV Tandetron accelerator in the University of Tsukuba. The experimental setup is similar to the one described in Ref. [2]. The proton beam passed through 2 collimators (each10 mm in diameter) and was focused on the target. The two collimators were located 50 and 100 cm up stream of the target. The solid targets were prepared from $^{6}Li_2O$ material evaporated onto a 0.2 mm thick Ta backing, with a thickness of 36 μg/cm^2. A high efficiency HPGe detector (GEM140P4-ST) was placed in close geometry at zero degree with respect to the beam direction. An ORTEC ULTRA ion-implanted silicon detector was installed at 135°.

From equation (1), we can give out the relationship between different energy points of E_1, E_2:

$$\frac{S(E_1)}{S(E_2)} = \frac{E_1}{E_2}\frac{N_1 Q_2}{N_2 Q_1}\frac{\exp(-2\pi\eta_2)}{\exp(-2\pi\eta_1)} \quad (3)$$

Here, N_1, N_2 are the counts of clover detector at different energy points, Q1, Q2 are the beam integrations of different energy points. Using this formula, we normalized our new experimental data at $E_{c.m.}$ = 206 keV, which was given in Ref. [2]. The preliminary result was shown in Fig.1. From plot we can see that our new data can consist with the previous result in large energy region. The little deviation at high energy point is due to the anisotropic angle distribution of γ-rays. A deeper analysis is still in process. More results will be reported in the future.

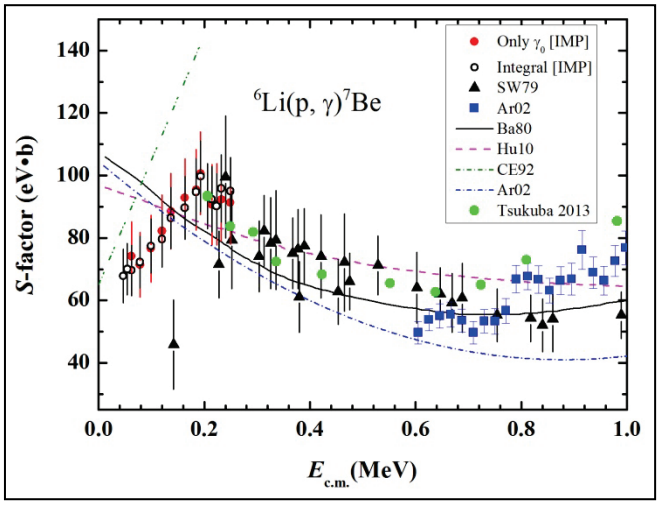

Fig.1. preliminary result of ^{6}Li(p, γ)^{7}Be

References

[1] C. Rolfs, W. Rodney. Cauldrons in the Cosmos. The University of Chicago Press, 1988.

[2] J.J. He, et al. Phys. Lett. B 725 (2013) 287.

[1] Institute of Modern Physics, Lanzhou, Gansu, China
[2] RIKEN Nishina Center, Hirosawa 2-1, Wako, Saitama 351-0198, Japan
[3] High Enegry Accelerator Reseach Oganiation (KEK), Oho 1-1, Tsukuba, Ibaraki 305-0801, Japan
[4] Japan Atomic Energy Agency, Shirakata Shirane 2-4, Tokai, Ibaraki 319-1106, Japan
[5] Center for Nuclear Study, University of Tokyo, Hirosawa 2-1, Wako, Saitama 351-0198, Japan
[6] Hoseo University, Chung-Nam 336-795, Korea
[7] Division of Theoretical Astronomy, National Astronomical Observatory of Japan, Osawa, Mitaka, Tokyo 181-8588, Japan

2.3 Development of a beam monitor detector using a mirror-electric field

D. Nagae, Y. Abe, S. Okada, K. Sawahata, Y. Saito, N. Inaba and A. Ozawa

The precision mass measurement system of rare RI is proposed at RIKEN RI beam factory [1]. In this plan, the mass is deduced from a time-of-flight of RIs in the ring. Details for the principle of the mass measurement are described elsewhere [2]. In order to monitor a motion of the stored rare RI in the ring, a dedicated detector has been developing. Required specifications and performances for the monitor detector are i) the effective area is consisted by thin material and have a large size match a beam size, ii) separation of the each revolution, and iii) position resolution less than 10 mm. To satisfy such the requirements, a beam monitor detector consisting of thin and large carbon foil, Micro Channel Plate (MCP) and using a electrostatic-mirror field has been developing. The principle of the monitor detector is that a beam generates secondary electrons in passing through a thin carbon foil. The secondary electrons are accelerated by an acceleration-electric field (E_{acc}) which is produced by a potential of carbon foil (V_{foil}) and that of acceleration grid (V_{acc}). Electrons are directed to the mirror-electric field comprising two parallel grids placed at 45 degree to the ion trajectory. Then they are deflected at 90 degree toward the MCP by a electrostatic mirror field (E_{mir}) which is produced by two parallel grids. The electrostatic-mirror field is express as $E_{\mathrm{mir}} = V_{\mathrm{out}} - V_{\mathrm{in}}$, where V_{out} and V_{in} denote a potential for outside grid of parallel grid and that for inside grid of parallel grid. The potential of inside grid is same as that for acceleration grid (V_{acc}). These grids are made of Au + W wires with a diameter of 40 μm and a pitch distance of 1 mm for the acceleration grid and that of 3 mm for the two parallel grids. A schematic view of the monitor detector is shown in Fig. 1. The size and thickness of the carbon foil is 100 mm $\times$ 50 mm and 60 μg/cm^2.

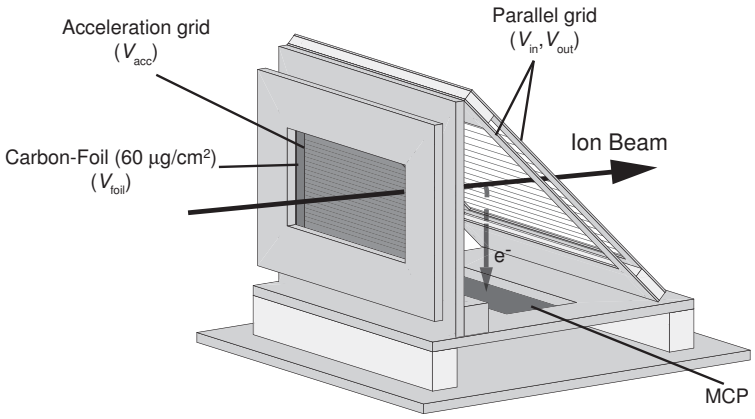

Fig. 1. Schematic layout of the monitor detector

An experiment to evaluate a performance of the detector was performed at SB2 beam line [3] in HIMAC. The experimental setup is shown in Fig. 2. ^{84}Kr beam ($\sim$ 170 MeV) was transported to the detector. In order to investigate the time resolution, a Time-Of-Flight(TOF) between a trigger detector and the monitor detector was measured. As the trigger detector, 1-mm-thick plastic scintillator of which both ends were connected on photomultiplier tubes was used. Two parallel plate avalanche counters (PPAC)

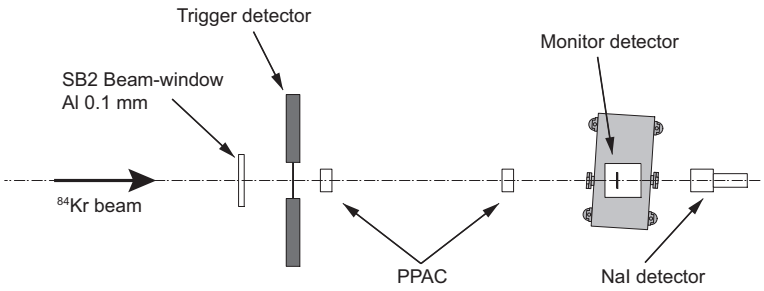

Fig. 2. Schematic layout of the monitor detector

were used to measure the position distribution of the beam and to obtain the beam profile at the carbon foil by a ray-trace technique.

In this measurement, the potentials were set as $V_{\mathrm{foil}} = -3250$ V, $V_{\mathrm{acc}} = V_{\mathrm{in}} = -2500$ V, and $V_{\mathrm{out}} = -4000$ V so as to the TOF spectrum was narrow. A typical TOF spectrum is shown in Fig. 3. The time resolution is obtained by fitting the TOF spectrum with a Gaussian function. The obtained width of the peak includes the intrinsic time resolution of the trigger detector, which is σ= 50 ps. By subtracting the contribution of the trigger detector, preliminary intrinsic time resolution was deduced as $\sigma \approx 130$ ps. The obtained detection efficiency is about 70%.

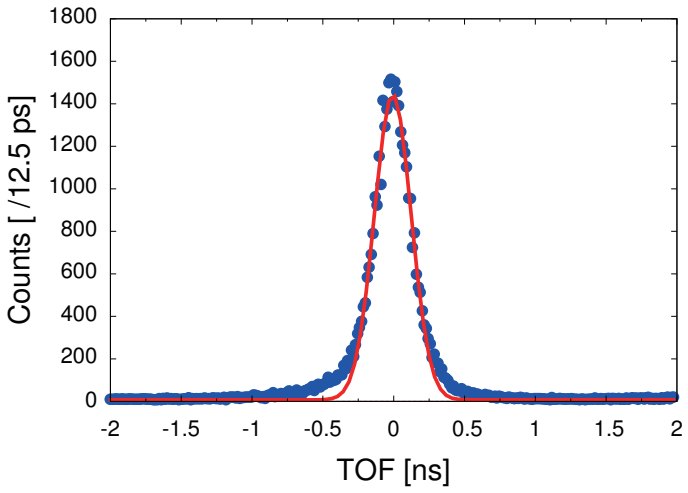

Fig. 3. TOF spectrum

References

[1] Y. Yano., Nucl. Instr. and Meth., **B261**, 1009(2007).

[2] Y. Yamaguchi et al., Nucl. Instr. and Meth., **B266**, 4575(2008).

[3] M. Kanazawa, et. al., Nucl. Phys., **A 74**, (2004) 393.

2.4 Test of rotating magnetic field system for β-NMR method

D. Nagae, Y. Ishibashi, N. Inaba, S. Okada, K. Sawahata, Y. Abe and A. Ozawa

A rotating magnetic field system has been developing [1, 2] to determine a sign of magnetic (μ) moment by the β-ray detected nuclear magnetic resonance (β-NMR) method [3]. Using the rotating magnetic field system, a measurement of the sign of the μ moment for proton has been conducted by a $\pi/2$ pulse NMR method and successfully confirmed the sign of the μ moment for proton [4].

In the present work a performance of the system was studied with spin-polarized ^{20}F ($I = 2^+$, $T_{1/2} =$ 11.163 s, $\mu(^{20}\mathrm{F}) = +2.09335(9)\ \mu_\mathrm{N}$) nuclei at the Research Center for Nuclear Physics, Osaka University. A spin-polarized ^{20}F was produced via nuclear-polarization transfer reaction with spin-polarized deuteron beam at $E = 10$ MeV on a 0.5-mm-thickness CaF_2 crystal. The CaF_2 crystal was mounted at a center of the β-NMR apparatus (see Fig. 1 (a)). A static magnetic field $B_0 = 290$ mT was applied to the crystal. The β rays emitted from ^{20}F nuclei were detected with scintillator telescopes located above and below the crystal. The up/down ratio R of the β-ray counts is written as $R_0 = a(1 + v/c \cdot A_\beta P)/(1 - v/c \cdot A_\beta P)$, where a denotes a constant factor representing asymmetries in counter solid angles and efficiencies, v and c are the velocity of the β particle and light. A_β and P denote the β-ray asymmetry factor and spin polarization. A rotating magnetic field perpendicular to the static field is applied to ^{20}F by using the two pairs of coils. If the frequency and the direction of the rotating magnetic field corresponds to the resonance one, the direction of the spin polarization is changed from P to $-P$ by the NMR. Thus the up/down ratio is changed as $R = a(1 - v/c \cdot A_\beta P)/(1 + v/c \cdot A_\beta P)$. When the polarization is altered due to the resonant spin change, a change appears in a ratio R_0/R. The β-ray asymmetry $A_\beta P$ is obtained as,

$$A_\beta P = \frac{\sqrt{(R_0/R)} - 1}{\sqrt{(R_0/R)} + 1}, \tag{1}$$

here, we took an approximation that $v/c \simeq 1$, since only a high-energy portion of the β particle was included in the analysis. The deuteron beam was pulsed with beam-on and -off periods of 16 and 22.02 s, respectively. In the beam-off period of a beam cycle, the RF magnetic field B_1 was applied for the first 10 ms duration. Then, the β rays were counted for 22 s, and in the last 10 ms of the beam-off period the B_1 field was applied again to restore the spin direction. At first we measured the R_0 without B_1 field and then measured the R with the B_1 field. This cycle were repeated until the sufficient measurement statistics were attained.

Figure 2 shows the measured $A_\beta P$ values for ^{20}F with the linear B_1 field 1, and 2, ,a right-circularly rotating B_1 field, and a left-circularly rotating B_1 field. A definition of the RF magnetic field is shown in Fig. 1 (b). The linear B_1 fields can be regarded as superpositions of right- and left-circularly rotating magnetic fields. Thus, the spin reversal is occurred when the frequency of the B_1 field is correspond to the resonant one. The frequency of these B_1 fields were swept from 2047.5 kHz to 2152.5 kHz during 10 ms. The $A_\beta P$ values of the linear B_1 fields are indicated the occurrence of the spin reversal. Considering the obtained $A_\beta P$ values, the asymmetry parameter of ^{20}F ($A_\beta = -1/3$), and the direction of B_0 (from up to down), the direction of the spin-polarization of ^{20}F was been determined as parallel to the B_0. The $A_\beta P$

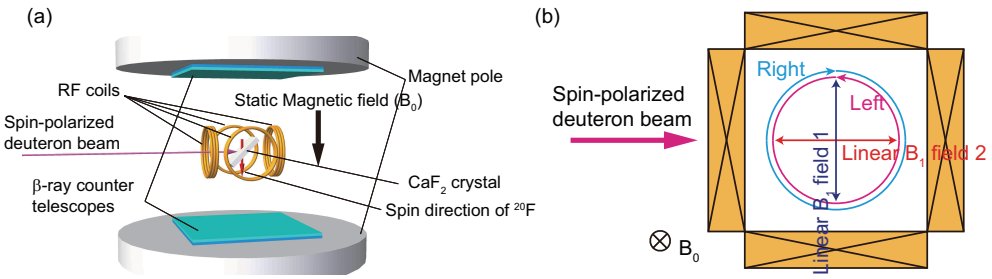

Fig. 1. (a) Schematic layout of the β-NMR apparatus, (b) Definition of RF magnetic fields

value with the left-circularly rotating B_1 field is clearly deviated from 0, while the value with the right-circularly rotating B_1 field is small. These results indicate that the sign of the $\mu(^{20}\mathrm{F})$ moment is positive. The obtained sign derived from this analysis is in agreement with the reported one [5].

In the present work, spin polarizations P of ^{41}Sc were measured. The spin-polarized ^{41}Sc was produced in a $^{40}\mathrm{Ca}(\vec{d},n)^{41}\vec{\mathrm{Sc}}$ at $E_{\vec{d}} = 20$ MeV. For the reaction target, two CaO pellets made from CaO powder, and from a $CaCO_3$ powder were used. The obtained Ps and previous result [6] are shown in Fig. 3. In the previous measurement, a CaO pellet made from CaO powder was used and the energy of the spin-polarized deuteron beam was set at $E_{\vec{d}} = 7$ MeV. While the polarizations of present work were maintained both CaO pellets, the values were extremely small compared with the previous value. These result suggest the spin-polarization is well transferred in a low energy reaction.

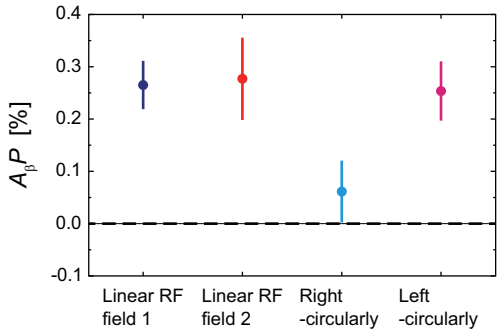

Fig. 2. Obtained $A_\beta P$ value of ^{20}F

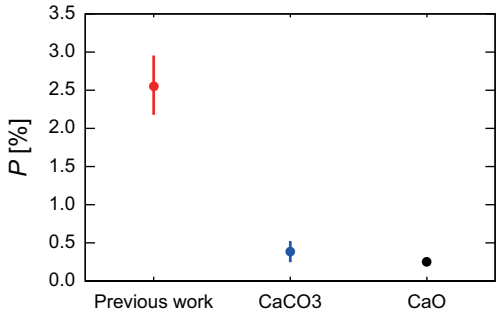

Fig. 3. Spin polarizations of ^{41}Sc

References

[1] T. Niwa et al., UTTAC annual report 2011, UTTAC-81, 5 (2012).

[2] D. Nagae et al., Hype. Int., **220**, 65 (2013).

[3] K. Sugimoto et al., J. Phys. Soc. Jpn. **21**, 213 (1966).

[4] D. Nagae et al., UTTAC annual report 2012, UTTAC-82, 7 (2013).

[5] N.J. Stone, Atomic Data and Nuclear Data Tables **90**, 75 (2005).

[6] Y. Ishibashi et al., UTTAC annual report 2010, UTTAC-80, 17 (2011).

3.

MATERIALS SCIENCE

3.1 Effect of synthesis conditions on magnetic properties of ferromagnetic iron oxide nanoparticles using Mössbauer spectroscopy

Akari Horiuchi, M. Kishimoto, H. Yanagihara and E. Kita

Modification of the physical properties of nanoparticles is greatly affected by shape, and thus controlling nanoparticle shape is an important issue. Shape especially influences the magnetic anisotropy. We have developed oval-shaped nano-platelets composed of ferromagnetic iron oxides smaller than 50 nm in size. The effect of reaction temperature on magnetic properties during dehydration is reported.

Ferromagnetic iron oxide nanoparticles were prepared as follows: first, α-FeOOH nano-platelets, used as precursor materials, were synthesized through precipitation and a hydrothermal treatment. Tetra-ethylene glycol (TEG) was used as a polyhydric alcohol for reducing the α-FeOOH nano-platelets. A dispersion of α-FeOOH nanoparticles and TEG was heated to several predetermined temperatures. We labeled the various nanoparticle samples as GTe260 through GTe300, corresponding to reaction temperatures between 260 and 300 °C. Magnetizations of dry powdered samples were measured using a vibration sample magnetometer (VSM). Crystal structures of the samples were obtained using X-ray diffraction (XRD). Mössbauer spectra for GTe290 were recorded at 4.2 K, 77 K, and room temperature. These spectra were numerically analyzed using fitting software (MössWinn 4.0).

Figure 1 shows the XRD patterns of samples obtained by heating α-FeOOH to various temperatures in the 260–300 °C range. Diffraction peak intensity corresponding to the spinel structure increased with increased reaction temperature. However, the peak originating from α-Fe_2O_3 became very faint in XRD patterns of GTe300.

Figure 2 shows the Mössbauer spectra of GTe290 recorded at 4.2 K, 77 K, and 295 K. The solid lines indicate the fitted results, which are summarized in Table 2. Three ferromagnetic sextets and a doublet with negligible area ratio (5.8%) reasonably fit the spectrum recorded at 295 K. The sub-spectrum with the highest hyperfine field (H_{hf}) value, 506 kOe, was attributed to the Fe^{3+} ions corresponding to α-Fe_2O_3. The sub-spectra with the second largest, 489 kOe, and smallest, 454 kOe, H_{hf} values were assigned to the Fe^{3+} ion in the A lattice and the $Fe^{2.5+}$ ion in the B lattice of Fe_3O_4, respectively.

Although GTe290 was characterized as a mixture of Fe_3O_4 and α-Fe_2O_3 nanoparticles, there remained a possibility that γ-Fe_2O_3 particles were partially mixed in as well. In order to confirm that GTe290 was a mixture of only Fe_3O_4 and α-Fe_2O_3, measurement was carried out at low temperature. Three ferromagnetic sextets fit the spectrum recorded at 4.2 K. The sub-spectrum with the highest H_{hf}, about 532 kOe, was attributed to the Fe^{3+} ions corresponding to α-Fe_2O_3. Those with the second largest, 510 kOe, and smallest, 467 kOe, H_{hf} were respectively assigned to the Fe^{3+} ion in the B lattice and the Fe^{2+} ion in the B lattice of Fe_3O_4, an inverse spinel structure with a cubic cell. Therefore, spinel-structured iron oxide obtained by heating α-FeOOH particle dispersions in TEG was identified as Fe_3O_4.

Table 1 shows the variation of the coercive force, saturation magnetization, and squareness against the reaction temperature. The coercive force remained nearly constant at 133–153 Oe irrespective of the reaction temperature. However, the saturation magnetization of the samples increased from 6.87 to

81.4 emu·g^{-1} as the reaction temperature increased.

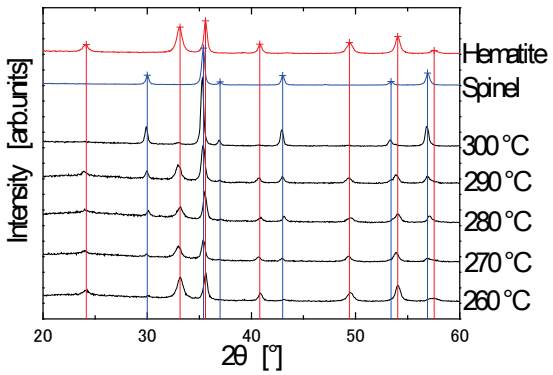

Figure 1. X-ray diffraction patterns of samples synthesized at different temperatures.

Table 1. Magnetic properties of samples synthesized at different temperatures.

sample	T [℃]	M_s [emu· g^{-1}]	H_c [Oe]	S
GTe260	260	6.87	145	0.26
GTe270	270	17.1	133	0.22
GTe280	280	28.8	146	0.23
GTe290	290	54.1	153	0.26
GTe300	300	81.4	150	0.33

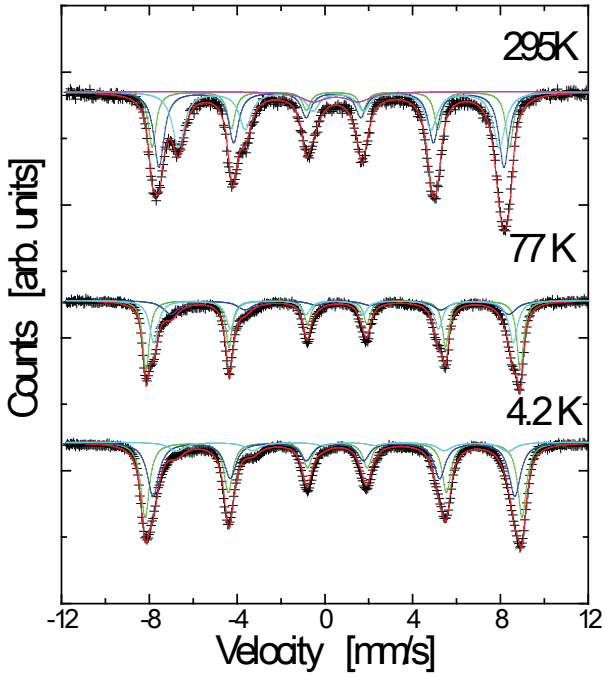

Figure 2. Mössbauer spectra of a sample synthesized at 290 °C.

Table 2. Mössbauer fitting parameters.

		H_{hf} [kOe]	IS [mm·s^{-1}]	QS [mm·s^{-1}]	Area ratio [%]	Ion	Crystal structure
295	F1	506	0.361	-0.174	21.8	Fe^{3+}	α-Fe_2O_3
	F2	489	0.349	-0.093	38.3	Fe^{3+}(A)	Fe_3O_4
	F3	454	0.621	0.027	34.2	$Fe^{2.5+}$(B)	Fe_3O_4
	D		0.504	2.052	5.80		
77		528	0.472	-0.187	43.7	Fe^{3+}	α-Fe_2O_3
		476	0.756	-0.143	20.7	Fe^{2+}(B)	
		507	0.415	-0.037	35.6		
4.2		532	0.485	-0.174	45.5	Fe^{3+}	α-Fe_2O_3
		510	0.438	-0.046	43.5	Fe^{3+}(B)	Fe_3O_4
		467	0.936	-0.291	11.0	Fe^{2+}(B)	Fe_3O_4

3.2 Conversion electron Mössbauer spectroscopy (CEMS) of cobalt ferrite thin films grown by sputtering using a ^{57}Fe enriched target

R. Aoyama, H. Yanagihara, Ko Mibu and E. Kita

High perpendicular magnetic anisotropy (PMA) materials have attracted attention because of their potential use in magnetic recording media and other practical applications. In addition to high PMA, materials that do not contain Pt, a rare metal, are ideal for the future uses to avoid resource issues such as scarcity. The magnetization and PMA of cobalt ferrite thin films, which are high PMA materials, change with composition and production conditions. As such, cobalt ferrite thin films are the subject of our study, and we have reported changes in their magnetization and PMA by changing their composition and production conditions [1].

In order to clarify the mechanism of anisotropy in cobalt ferrite thin films, the electronic and magnetic states should be studied using Mössbauer spectroscopy. However, it is not possible to detect these electronic and magnetic states via transmission through the sample in thin films grown on thick substrates. Conversion electron Mössbauer spectroscopy (CEMS) can be used on such samples because the electrons emitted back from the surface are detected. However, it takes a long time to gather CEMS results from samples thinner than 100 nm because of the insufficient amount of ^{57}Fe nuclei in cobalt ferrite thin films. ^{57}Fe enrichment is a well-known technique to decrease measurement time, but ^{57}Fe enriched RF sputtering targets are expensive to produce. To solve this problem, we prepared a locally enriched ^{57}Fe target.

Figure 1 shows the schematic illustration of the locally ^{57}Fe enriched target system. The system was composed of a 1 mm thick doughnut shaped ^{57}Fe enriched disk, covering the erosion part of sputtering, and a natural Fe base plate. Cost was reduced by shrinking the area of the enriched disk and lowering the quantity of ^{57}Fe used to 25% of the disk material. Cobalt ferrite thin films for CEMS were grown on a MgO(001) single crystal substrate by co-sputtering using a locally enriched ^{57}Fe target and Co target. The O_2 flow rate was set to 7 sccm and the substrate temperature was fixed at 300 ºC during sputtering.

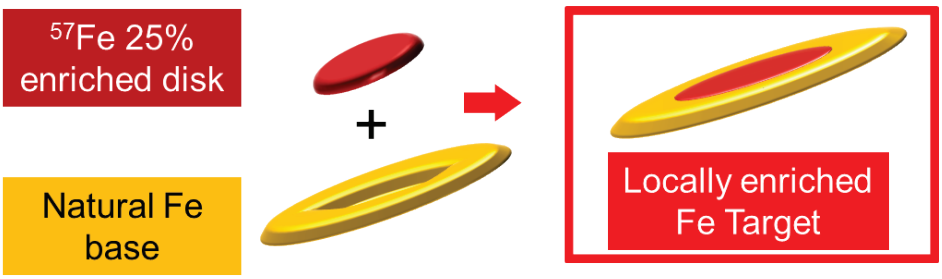

Figure 1. Schematic of a locally enriched ^{57}Fe target for RF sputtering.

Figure 2 shows a CEMS spectrum for a $Co_{0.65}Fe_{2.35}O_4$ thin film. The time to collect data of equivalent quality was ideally shortened by a factor of ten because the amount of ^{57}Fe was 25% in the

enriched target compared to 2.3% in natural Fe. Data collected for 16 hours is shown in Figure 2, and the spectrum has a distinct enough signal to noise ratio for detailed discussion. The enriched ^{57}Fe combination target enabled us to shorten measuring time drastically and will be a powerful tool in analyzing the magnetic state of Fe based thin films.

The spectrum was fit to a combination of three ferromagnetic sub-spectra, and the fitting parameters, hyperfine field (H_{hf}), isomer shift (IS) and quadrupole split (Q.S.) are listed in Table I. The spectrum was fairly symmetric and the isomer shifts were 0.3–0.4 mm/s and were fairly similar to those of trivalent Fe ions. It was supposed that about 15% (= 0.35/2.35) of Fe atoms should be in the divalent state, however, it is not clearly seen in the spectrum. This suggested that the film was well oxidized and the number of divalent Fe atoms was small. Sites with small hyperfine fields (site 1) may be attributed to the surface Fe atoms.

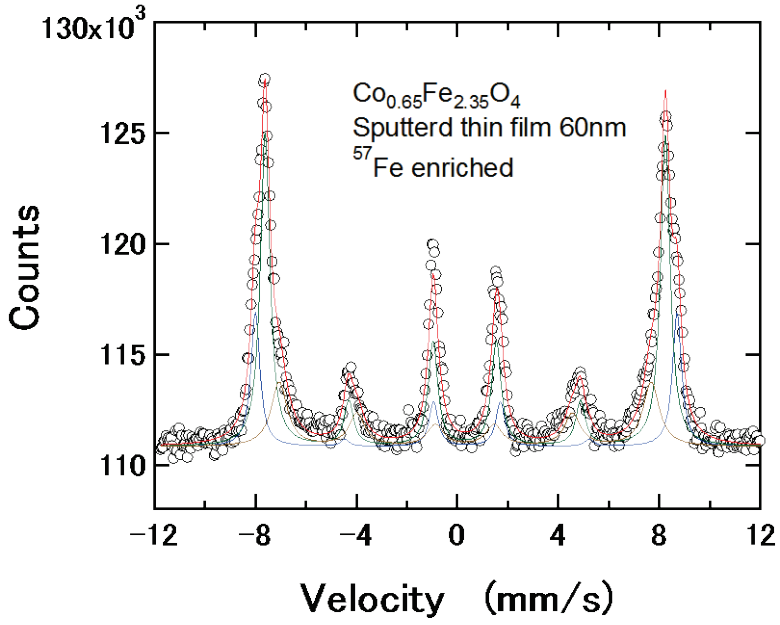

Figure 2. Conversion electron Mössbauer spectroscopy (CEMS) spectrum for a $Co_{0.65}Fe_{2.35}O_4$ thin film recorded at 300 K. Solid lines indicate fitted results.

Table I. Mössbauer fitting parameters for a $Co_{0.65}Fe_{2.35}O_4$ thin film

Sub-spectrum	H_{hf} (kOe)	IS (mm·s^{-1})	Q.S. (mm·s^{-1})	Area (%)	Ion (site)
F1	426.0	0.307	0.020	23.51	Fe^{3+} (?)
F2	458.5	0.305	0.024	54.60	Fe^{3+} (B)
F3	482.8	0.365	-0.019	21.89	Fe^{3+} (A)

References

[1] T. Niizeki, Y. Utsumi, R. Aoyama, H. Yanagihara, J. Inoue, Y. Yamasaki, H. Nakao, K. Koike, and Eiji Kita, Appl. Phys. Lett., **103**, 162407 (2013). **104**, 059902 (2014) [erratum].

3.3 Magnetic states of ion implanted Fe_3O_4 thin films studied by Mössbauer spectroscopy

Eiji Kita, K.Z. Suzuki, Yang Liu, Y. Utsumi, J. Morishita. T. Niizeki, K. Mibu and H. Yanagihara

Oxide ferro-/ferrimagnetic materials have been investigated for many years and have tremendous potential for use in various applications such as high-density recording media and spintronic devices. Recently, we fabricated spinel-type oxide thin films using RF sputtering and found strong perpendicular magnetic anisotropy energy on the order of 10 Mergs/cm^3 in Co ferrite thin films grown on MgO(001) substrates [1]. These materials have potential as magnetic recording media, and one practical application is the use of nanoscale patterning in high-density recording media. Bit-patterned media (BPM) have emerged as the dominant candidate for developing ultra-high density hard disk systems [2]. Recently, as the first step toward pattern formation of spinel type ferromagnetic oxides, we investigated the effectiveness of controlling the magnetism of a typical spinel ferromagnetic oxide, Fe_3O_4, via N_2 and Kr ion implantation [3,4]. Mössbauer study on the effect of Kr irradiation on Fe_3O_4 thin films is reported.

Ferrite thin films were prepared using reactive sputtering, introducing O_2 gas into Ar base gas during film growth in an RF planner magnetron sputtering apparatus [5]. An Ar gas flow of 30 sccm was introduced, and the O_2 flow was controlled at 0.5 sccm. Cleaved MgO(001) single crystals were used as substrates. Sputter deposition was performed at the substrate temperature of 300 °C and 13-nm-thick thin films were obtained for magnetization measurements. For Mössbauer studies, thin films with a thickness of 13 nm were fabricated in the same manner as other samples by using the ^{57}Fe enriched Fe_3O_4 target system [6]. The Fe_3O_4 films were covered with a carbon layer of around 10 nm prior to ion irradiation. Kr ions were accelerated by a conventional ion implantation system. The acceleration voltages (Vacc) was set to 30 kV, and the dosages of ions were controlled from 1×10^{14} to 6×10^{15} ions/cm^2. The Mössbauer study was carried out using standard conversion electron Mössbauer spectroscopy.

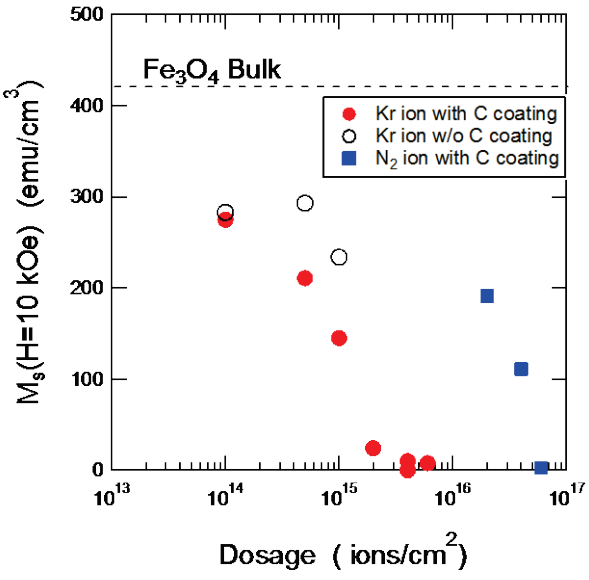

Fig. 1. Dependence of saturation magnetization, Ms, on Kr ion implantation, for three Fe_3O_4 sputtered thin films. Solid circles and open circles show the magnetization for the samples with C coated and without C coated layer, respectively. Closed squares show the magnetization of the sample with C coated layer irradiated by N_2 ions.

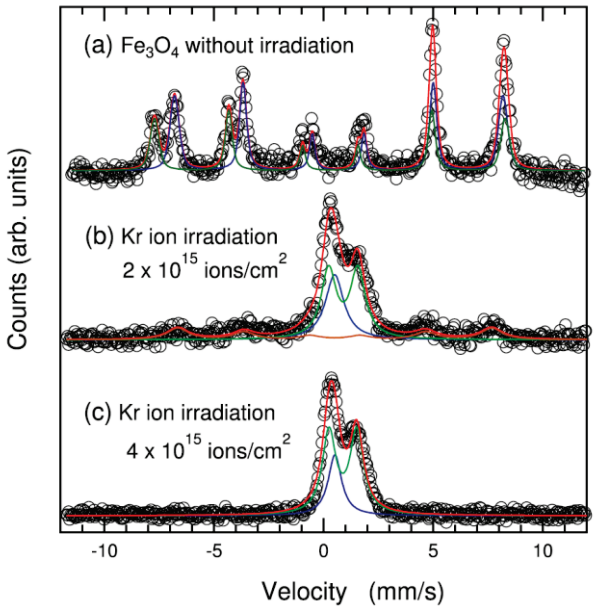

Fig. 2. CEMS spectra recorded at 300 K.

The Mössbauer spectra of the Fe_3O_4 thin films with Kr-irradiation treatments of (b) 2×10^{15} ions/cm^2 and (c) 4×10^{15} are in Fig. 2. Magnetization levels of 200 and 0 emu/cm^3 were achieved for samples (b) and (c), respectively. The spectrum of the low-irradiation sample in (b) was fitted to the combination of a weak broad magnetic sextet, a non-magnetic doublet, and a non-magnetic singlet. The spectrum for a 50 nm thick Fe_3O_4 film without irradiation is plotted as a reference in Fig. 2 (a) and was fitted to the combination of two magnetic subspectra with bulk parameters. The ferromagnetic component has a hyperfine field of 445 kOe and an isomer shift of 0.50 mm/s which are almost comparable to those of Fe^{3+} ions and wide line widths. The area ratio of a ferromagnetic component is roughly estimated to be 23%, and this agrees qualitatively with the value of saturation magnetization.

A further increase in irradiation ions resulted in the disappearance of the ferromagnetic component of (b), and the paramagnetic components can be fitted by using the same parameters as those for sample (b). There are no intermediate subspectra with smaller hyperfine fields than those shown in the spectra of (b). Our results imply two-phase separation and absence of any intermediate phase in the irradiated sample, thereby suggesting that the transition of Fe_3O_4 from ferromagnetic to paramagnetic phases occurred sharply due to Kr ion irradiation.

References

[1] T. Niizeki, *et al*.,, Appl. Phys. Lett., **103**, 162407 (2013). **104**, 059902 (2014) [erratum].

[2] B. D. Terris and T. Thomson, J. Phys. D: Appl. Phys., 38, R199 (2005).

[3] Eiji Kita, *et al*., Jpn. J. Appl. Phys. **53** (2014) 020306.

[4] Eiji Kita, *et al*., J. Appl. Phys., **115** (2014) 17B907.

[5] H. Yanagihara, *et al*., J. Phys. D: Appl. Phys. **46**, 175004 (2013). **47**, 129501 (2014) [erratum].

[6] R. Aoyama, H. Yanagihara, K. Mibu and E. Kita, UTTAC Annual report 2013.

3.4 Mössbauer study of $Co_xFe_{4-x}N$ films grown by molecular beam epitaxy

K. Ito, T. Sanai, Y. Yasutomi, E. Kita and T. Suemasu

$Co_xFe_{4-x}N$ are promising ferromagnetic materials for application to spintronics devices due to their large spin-polarization of density of states at the Fermi level (P_D) [1-3]. Co_3FeN is expected to have larger $|P_D|$ of 0.75 ($P_D < 0$) than that of Fe_4N when Fe atoms are located at the corner (I) sites, and Co atoms at the face-centered (II) sites in the anti-perovskite unit cell (Fig. 1). X-ray magnetic circular dichroism (XMCD) measurements were performed on the epitaxial Co_3FeN film, and deduced spin magnetic moments of Fe and Co atoms in the Co_3FeN film were very close to those reported in Fe_4N and Co_4N, respectively [4]. It was suggested that Fe and Co atoms in the Co_3FeN film were located at both I and II sites. In this study, we evaluated the atomic sites of Fe atoms in epitaxial Fe_4N, $CoFe_3N$, and Co_3FeN films using conversion electron Mössbauer Spectroscopy (CEMS).

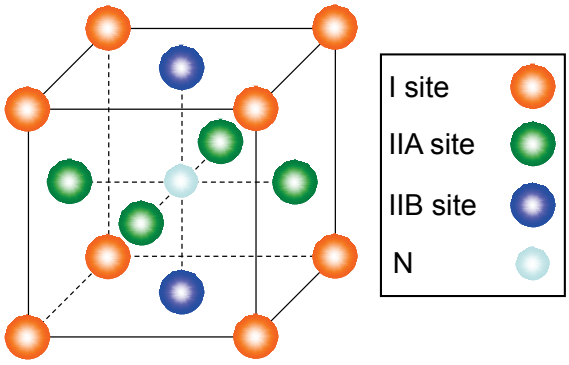

Fig. 1 Lattice structure of anti-perovskite nitride.

We performed CEMS measurements at room temperature for 19-nm-thick Fe_4N (sample A), 25-nm-thick $CoFe_3N$ (sample B), and 74-nm-thick Co_3FeN (sample C) films grown on $SrTiO_3(001)$ substrates by molecular beam epitaxy, supplying ^{57}Fe enriched (20%) solid iron and radio-frequency nitrogen plasma, simultaneously at 450 ºC. The velocity and isomer shift were calibrated using a standard spectrum of α-Fe. Obtained Mössbauer spectra were analyzed using commercially available fitting software, MössWinn 4.0.

Figures 2(a)-2(c) show the CEMS spectra for samples A-C, respectively. Obtained CEMS spectra were decomposed into three ferromagnetic components and one nonmagnetic component. We consider that the nonmagnetic component is attributed to the surface oxidized layer. The values of a hyperfine field, an isomer shift, and a quadrupole splitting of sample A were in good agreement with those reported [5]. However, the relative area ratio of I : II sites was not an ideal value of 1 : 3, but 0.53 : 3. The in-plane lattice parameter of the Fe_4N layer in sample A deduced from x-ray diffraction measurements was 0.3812 nm and is almost the same as that of the bulk value (0.3795 nm) [5]. Thus, we believe that this extremely-small occupation value for I sites is not attributed to Fe vacancies, but to the excess insertion and/or site-disorder of the N atoms since I sites are equivalent to II sites when the N atoms are located at interstitial sites between the two nearest I sites. The results of CEMS measurements for samples B and C also indicated that Fe atoms in samples B and C are located at both I and II sites and/or there is the site-disorder of the N atoms. This is consistent with our previous report [4]. This trend is also theoretically supported by the first-principles calculation, which shows that Co atoms tend to occupy both the I and II sites in $Co_xFe_{4-x}N$ from the view point of total energy [6]. In order to obtain highly spin-polarized $Co_xFe_{4-x}N$, optimization of the growth conditions is required to prevent the site-disorders.

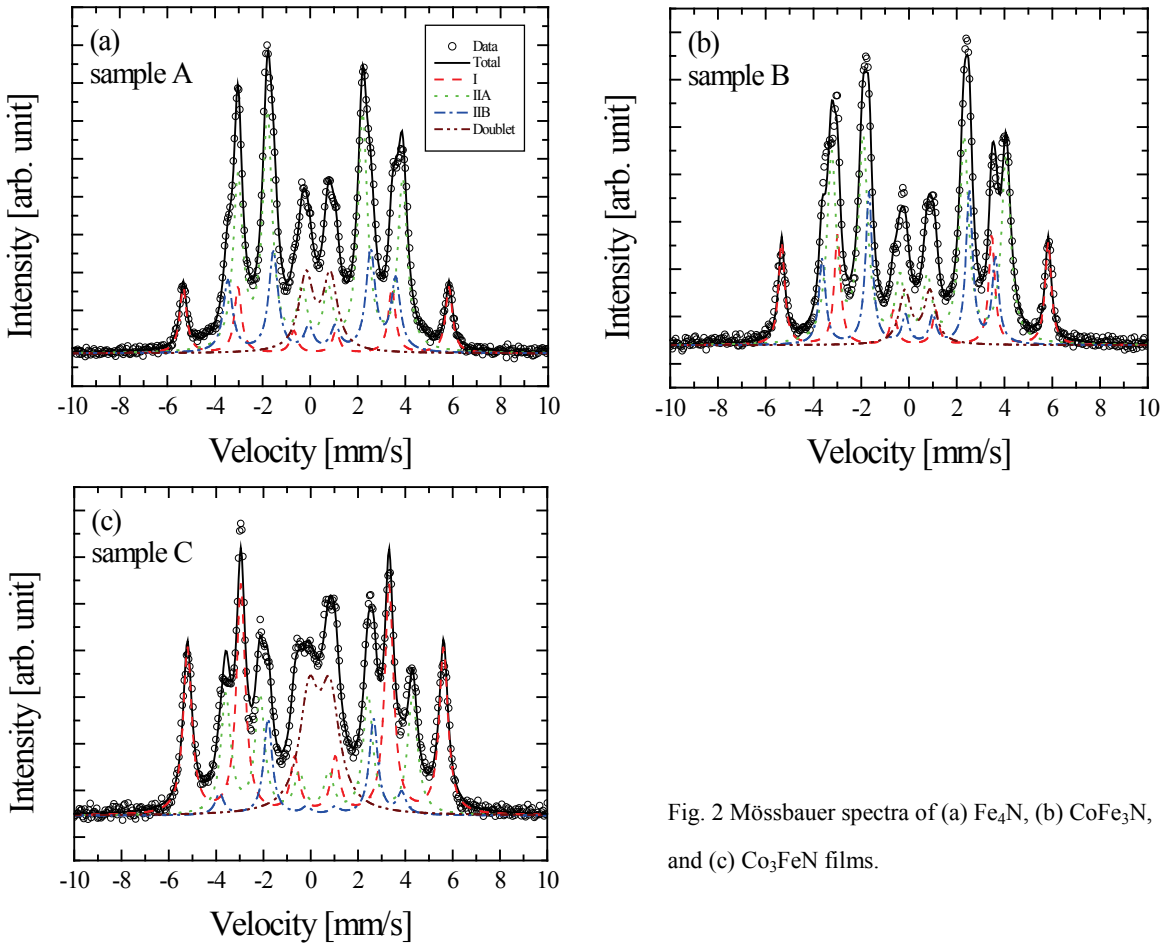

Fig. 2 Mössbauer spectra of (a) Fe_4N, (b) $CoFe_3N$, and (c) Co_3FeN films.

References

[1] S. Kokado, N. Fujima, K. Harigaya, H. Shimizu, and A. Sakuma, Phys. Rev. B **73**, 172410 (2006).

[2] Y. Imai, Y. Takahashi, and T. Kumagai, J. Magn. Magn. Mater. **322**, 2665 (2010).

[3] Y. Takahashi, Y. Imai, and T. Kumagai, J. Magn. Magn. Mater. **323**, 2941 (2011).

[4] K. Ito, T. Sanai, S. Zhu, Y. Yasutomi, K. Toko, S. Honda, S. Ueda, Y. Takeda, Y. Saitoh, Y. Imai, A. Kimura, and T. Suemasu, Appl. Phys. Lett. **103**, 232403 (2013).

[5] J. C. Wood and A. J. Nozik, Phys. Rev. B **4**, 2224 (1971).

[6] P. Monachesi, T. Björkman, T. Gasche, and O. Eriksson, Phys. Rev. B **88**, 054420 (2013).

3.5 Cluster effect on the yield of secondary electrons produced by inner shell electron excitation

S. Tomita, Y. Shiina, S. Tamura, R. Kinoshita, S. Ishii and K. Sasa

The generation rate of scattered electrons is generally assumed to be proportional to the inelastic stopping power because of the observed proportionality between the secondary electron yield and the stopping power [1]. However, it is experimentally shown that the proportionality does not hold for the case of fast carbon cluster ions. The secondary-electron yield for 0.5 MeV/atom C_4^+ ions is approximately 50% of that of atomic ions with the same velocity [2], whereas the electronic stopping power of C_4^+ is approximately the same as that of four atomic ions [3]. There must be a specific mechanism that reduces the secondary-electron yield despite of the same energy deposit. To investigate this problem further, we measured the molecular effect on the yield of secondary electrons which stem from close collisions in a first-excitation process.

The experiments were conducted at Tandem Accelerator Complex at the University of Tsukuba (UTTAC). A schematic of the experimental apparatus is shown in Fig.1. The accelerated molecular ions impinged on a thin carbon foil after passing through an aperture of 1 mm in diameter. The carbon foil was set with an angle of 45° with respect to the direction of fast ion beams. The foil was purchased from Arizona Carbon Foil Co., whose nominal thickness was 5 μg/cm^2. The ions that penetrated through the carbon foil were detected by an ion-implanted-silicon charged particle detector (ORTEC ULTRA). The opening angle of the detector was 1.6°, which was limited by a tiny aperture placed in front of the detector. The individual atoms scattered more than 1.6° by close collision with a target atom were not detected by the detector. The secondary electrons produced in backwards by a fast-molecule impact were extracted towards a micro channel plate (MCP) detector. The MCP signal was amplified with a charge-sensitive preamplifier and recorded with an ADC coincident with a signal from SSD event by event, using CAMAC data acquisition.

The coincident measurement with the projectile atoms allows us to measure backward secondary-electron yields as a function of the number of detected atoms. The mean values of secondary-electron yields are shown in Fig. 2 together with the results of single carbon atom impacts, $\gamma_i\left(\mathrm{C}^+\right)$ $(i = 0, 1)$.

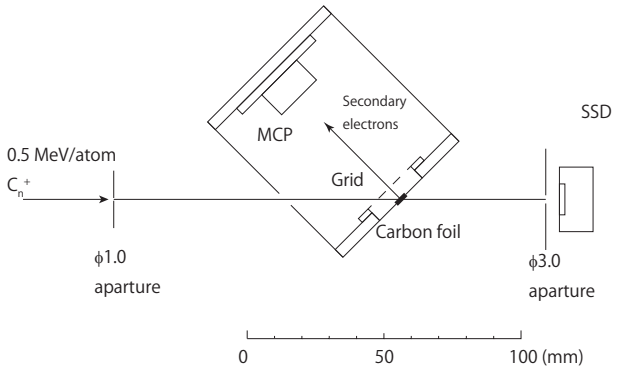

Fig. 1. Schematic drawing of experimental apparatus.

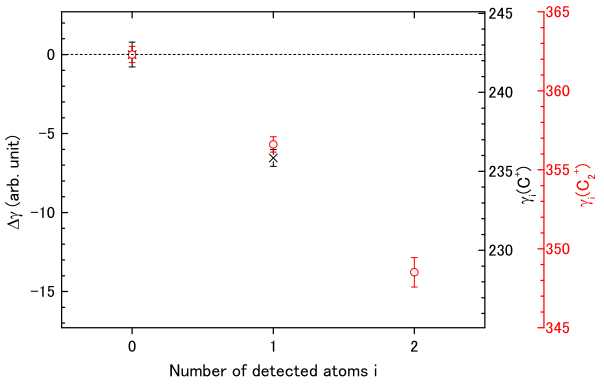

Fig. 2. Secondary electron yields for C_2^+, $\gamma_i\left(C_2^+\right)$, (open circles) and C^+, $\gamma_i\left(C^+\right)$, (crosses) as a function of the number of detected projectile atoms i. $\Delta\gamma$ shows the difference in secondary electron yields from that of the case that no constituent projectile atom was detected by the silicon detector.

The yields for both cases are plotted together to show the difference from the case that no projectile atoms were detected by silicon detector; therefore, the total yield of secondary electrons is shown on a different axis. It is clear that the secondary-electron yield decreases with the number of detected atoms. This can be reasonably understood as a contribution of inner shell electron excitation, similar to the case reported by Ogawa et. al. [4] for proton impacts. The classical trajectory calculation with Moliére potential results a closest distance of 0.02 Åfor a scattering angle of 1.6°, which is much smaller than the radius of 0.092 Åwhere the K-shell electron density of a carbon atom has its maximum value [5].

Note that there seems to be no molecular effect on the contribution of inner shell electron excitation, whereas total secondary electron yields are strongly suppressed. These results can be generally described as that there is no molecular effect in the phenomena involving violent collisions, such as inner-shell electron excitation in the present case. The enhancement for inner shell excitation stems from single-electron excitation, i.e., it excludes collective excitation such as plasmon excitations. However, it is difficult to conclude that the cluster effect occurs in a collective excitation.

References

[1] H. Rothard, K. Kroneberger, A. Clouvas, E. Veje, P. Lorenzen, N. Keller, J. U. Kemmler, W. Meckbach, and K.-O. Groeneveld. *Physical Review A*, 41:2521, 1990.

[2] S. Tomita, S. Yoda, R. Uchiyama, S. Ishii, K. Sasa, T. Kaneko, and H. Kudo. *Physical Review A (Atomic, Molecular, and Optical Physics)*, 73:060901, 2006.

[3] S. Tomita, M. Murakami, N. Sakamoto, S. Ishii, K. Sasa, T. Kaneko, and H. Kudo. *Physical Review A*, 82:044901, 2010.

[4] H. Ogawa, H. Tsuchida, and N. Sakamoto. *Physical Review A*, 68:052901, 2003.

[5] J. P. Desclaux. *Atomic Data and Nuclear Data Tables*, 12:311, 1973.

3.6 Limit of detection for hydrogen by developed high-resolusion ERDA system

D. Sekiba[1], K. Chito[1], I. Harayama[1], Y. Watahiki[1], S. Ishii[1] and K. Ozeki[2]

Recently we have developed high-resolution ERDA system on the D-course of the 1 MV Tandetron accelerator in UTTAC (University of Tsukuba, Tandem Accelerator Complex). The system is optimized to detect the hydrogen in the surface and subsurface of solids, taking into account the design of K. Kimura et al. of Kyoto University [1]. The analyzer consists of 90 degree sector lens and PSD (position sensitive detector) with MCP (micro channel plate made by Hamamatsu Photonics K.K.). While high-resolution ERDA with the sector lens demonstrates the nice depth resolution (~ 0.28 nm for the Si substrate), the detection limit for hydrogen is not good enough compared to that of SIMS (Secondary Ion Mass Spectroscopy) ~ 10^{18} particle/cm^3. The detection limit of analysis is generally determined by an intrinsic background produced by the detection system itself. In the case of ion beam analysis with sector lens and PSD, the origins of the background are mainly dark current of MCP and stray particles. Hashimoto et al. recently tried the system, which distinguishes the dark current and/or real signals, taking the coincidence of ion detection and secondary electron detection by means of two MCP [2,3]. There 200 ppm for As in the Si substrate with the data acquisition time of 1000 s for RBS (Rutherford Backscattering Spectroscopy) and 0.08 at.% B in the Si substrate for ERDA were achieved. On the other hand, the detailed detection limit of high-resolution ERDA for hydrogen has never been reported. We show the result of detection limit analysis for hydrogen with high-resolution ERDA employing a-C:H (hydrogenized amorphous carbon) film.

The 500 keV $^{16}O^+$ beam was shaped to 1 mm square with a four-quadrant slit and was irradiated onto the sample. The typical beam current was the several tens nA. The recoil angle was set at 30 degree from the beam incident direction. The dimension of the detection system is the same reported in Ref [2]. A thin Mylar foil (0.5 μm thickness) was put in front of the MCP to remove the forward scattered incident particles (^{16}O). The coincidence system reported in Ref. [2,3] was not used in the present study. The sample, a-C:H film (~150 nm thickness) deposited on Si(100) by chemical vapor desorption, was prepared by K. Ozeki in Ibaraki University. The contained hydrogen amount was carefully determined by means of conventional ERDA with the condition previously reported [4]. As a result, the composition ratio of hydrogen and heavy hydrogen in a-C:H were estimated as H : D : C = 33.1 : 11.5 : 55.4. By using SRIM code, the concentration of hydrogen in the sample was determined as 7.05 x 10^{22} particles/cm^3.

Figure 1(left) shows the high-resolution ERDA spectra taken on the above described sample. The surface peak is observed at ~ 500 ch indicating the adsorbed water on the surface. The edges at ~ 150 ch and 830 ch are artifacts due to the edges of MCP. To determine the limit of detection of hydrogen from Fig. 1, the counts of signal and background were integrated in the regions of 300 ch ~ 400 ch and 500 ch ~ 600

[1]UTTAC, Univ. of Tsukuba, Tennodai 1-1-1, Tsukuba, Ibaraki 305-8577, Japan
[2]Department of Mechanical Engineering, Ibaraki Univ. Nakanarusawa 4-12-1, Hitachi, Ibaraki 316-8511, Japan

ch. According to the simple definition suggested by Hashimoto et al. [2,3], the limit of detection for hydrogen with this system was estimated as 1.6 x 10^{20} particles/cm^3 with the data acquisition time of 308 s. The beam irradiation necessary for this measurement was 2.2 μC.

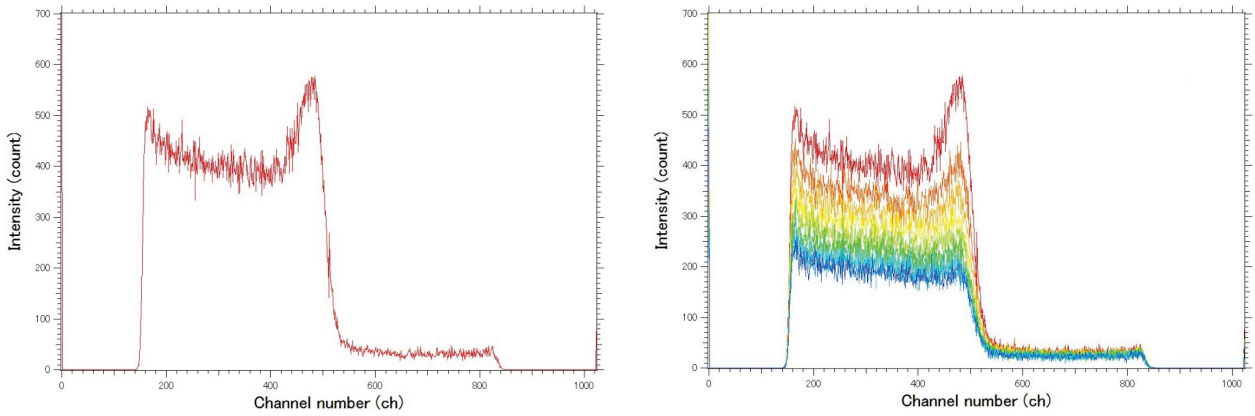

Figure1: (left) The high-resolution ERDA spectrum taken on a-C:H film with the 500 keV $^{16}O^{+}$ beam. The sample surface corresponds to ~ 500 ch, while the edges at ~ 150 ch and ~ 830 ch indicate the edges of MCP. (right) The change of the spectrum feature of high-resolution ERDA on a-C:H due to the damage. The spectra were taken with every ~2.2 μC.

Interestingly the contribution of stray particles, in this case mainly hydrogen scattered by inner wall of the chamber, was observed in Fig. 1(right). The spectra in Fig. 1(right) were taken with every ~ 2.2 μC on the same position of the sample. The intensity corresponding to the hydrogen concentration was continuously decreases indicating the desorption of hydrogen due to the beam irradiation damage. Accompanying the decrease of the signal intensity in the subsurface region, the intensity of background seen in the vacuum region also is suppressed. This implies that the stray hydrogen ions, which recoils from the subsurface and bulk, are not negligible compared to the dark current of MCP, when the sample is thick enough and contains a lot of hydrogen. In fact, in the case of thin oxide film (~ 4 nm) on SiC which contains much less hydrogen in bulk, we obtained a better limit of detection for hydrogen ~ 2.8 x 10^{19} particles/cm^3.

As a future work the development of a system, which can distinguish not only the dark current of MCP but also the stray recoil particle, will be necessary to take the further improvement of limit of detection in high-resolution ERDA.

References

[1] K. Kimura, K. Nakajima, H. Imura, Nucl. Instr. and Meth. B 140 (1998) 397-401.

[2] H. Hashimoto, K. Nakajima, K. Sasakawa, K. Kimura, Rev. Sci. Instrum. 82 (2011) 063301.

[3] H. Hashimoto, S. Fujita, K. Nakajima, M. Suzuki, K. Sasakawa, K. Kimura, Nucl. Instr. and Meth. B 273 (2012) 241-244.

[4] D. Sekiba, M. Horikoshi, S. Abe, S. Ishii, J. Appl. Phys., 106 (2009) 114912-1-5.

4.

ACCELERATOR MASS SPECTROMETRY

4.1 Depth profiles of ^{129}I and ^{129}I / ^{127}I ratio in soil at the near-field site of the Fukushima Dai-ichi Nuclear Power Plant

T. Matsunaka, K. Sasa, K. Sueki, T. Takahashi, M. Matsumura, Y. Satou, N. Shibayama, J. Kitagawa[1], N. Kinoshita[2], and H. Matsuzaki[3]

Massive nuclear fission products such as radioiodine were deposited on the surface in Fukushima via radioactive plume derived from the Fukushima Dai-ichi Nuclear Power Plant (FDNPP) accident. In order to evaluate inventory and penetration of accident-derived ^{129}I in the highly-contaminated area, depth profiles of ^{129}I concentration and ^{129}I / ^{127}I ratio in 5-cm-long soil cores after the accident were investigated at three sites shown in Fig.1: NM-6 site at Namie town (7.5 km northwest site from the FDNPP), Iw-2 site at Okuma town (4.3 km west site from the FDNPP) and Iw-8 site at Okuma town (8.2 km west site from the FDNPP).

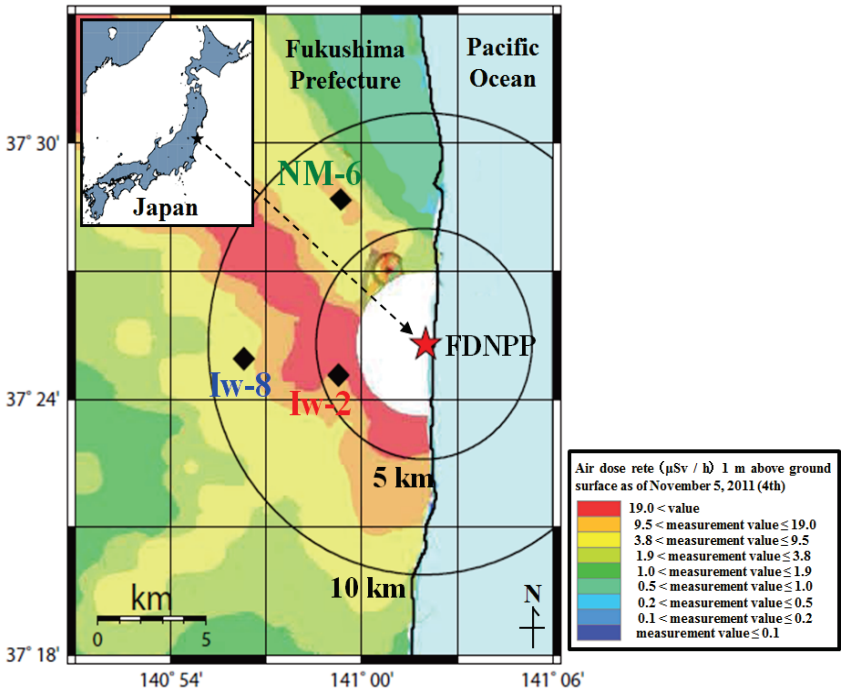

Fig.1. Sampling sites of 5-cm-long soil core within 10 km from the FDNPP on the distribution map of radiation dose as of November 5, 2011 (4th) mapping by MEXT.

Total ^{129}I inventories in the soil cores were estimated to be 1.80 Bq m^{-2} at NM-6, 1.84 Bq m^{-2} at Iw-2 and 0.68 Bq m^{-2} at Iw-8. Average ^{129}I / ^{127}I ratio in each soil cores after the accident (NM-6: 8.6×10^{-7}, Iw-2: 2.1×10^{-6}, Iw-8: 4.2×10^{-7}) shows typical ratios of the contaminated surface soils in Fukushima ($1.5 \times 10^{-8} - 7.2 \times 10^{-6}$) [1]. Therefore, accident-derived ^{129}I deposited at NM-6 and Iw-2 were 2.7 times higher than that at Iw-8. Depth profiles of ^{129}I concentration and ^{129}I / ^{127}I ratio exponentially declined with depth (Fig.2). Approximately 90% of deposited ^{129}I in 5-cm-long soil cores were observed in the surface

[1] Radiation Science Center, High Energy Accelerator Research Organization
[2] Institute of Technology, Shimizu Corporation
[3] MALT, The University of Tokyo

layer of 16.1 – 17.8 kg m^{-2} (1.6 – 2.5 cm) in depth. In addition, the relaxation mass depths (h_0) of ^{129}I were determined to be 8.2 kg m^{-2} at NM-6, 9.5 kg m^{-2} at Iw-2 and 9.2 kg m^{-2} at Iw-8.

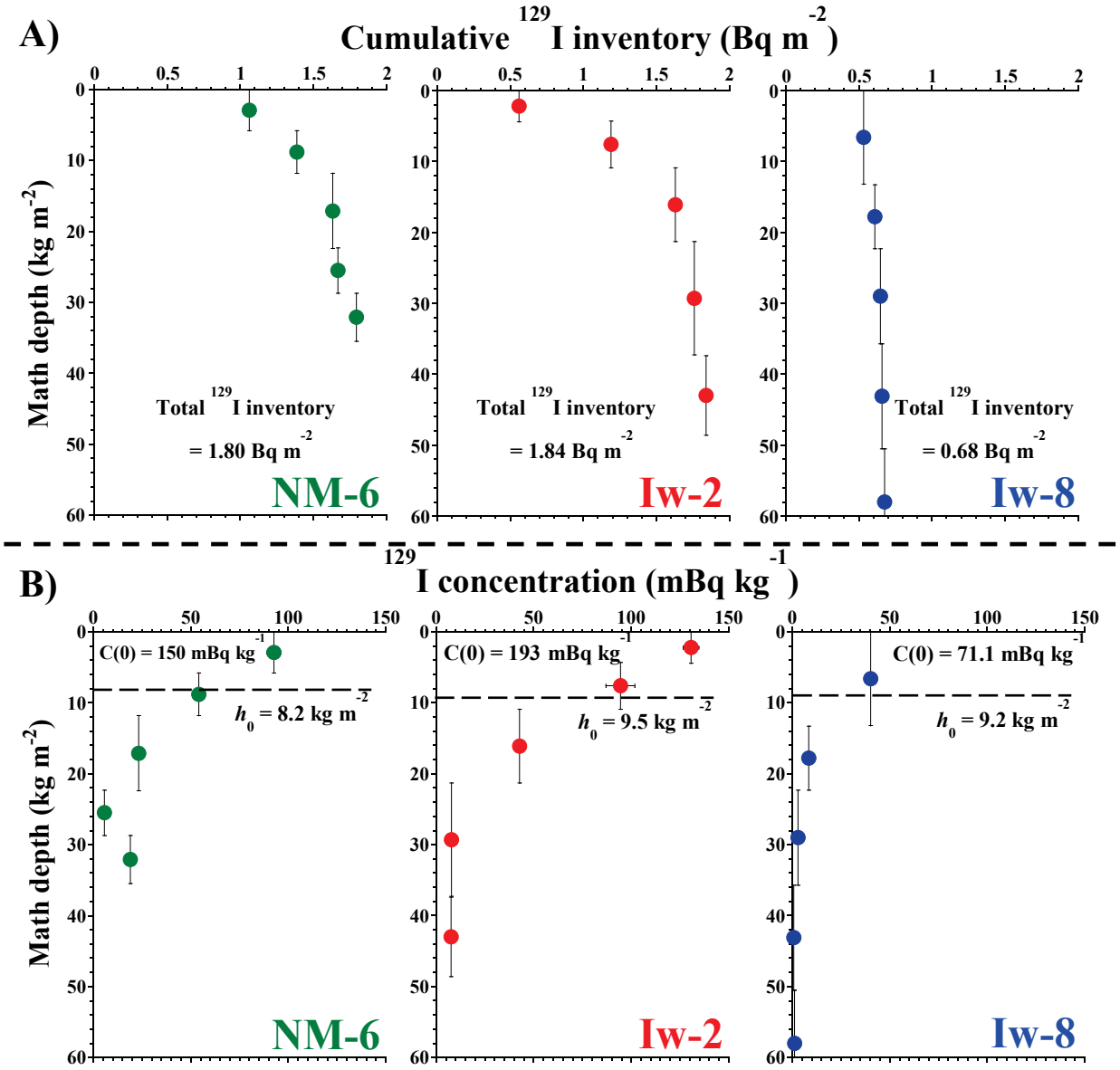

Fig.2. Cumulative ^{129}I inventories (A) and depth profiles of ^{129}I concentrations (B) in 5-cm-long soil core from NM-6, Iw-2 and Iw-8. Total ^{129}I inventories in the core, estimated activity ^{129}I concentration of surface soil (C(0)) and relaxation mass depth (h_0) of ^{129}I are shown in the profiles.

References

[1] Miyake et al. (2012) Geochemical Journal, 46, 327-333.

4.2 Study on monitoring of volcanic activity using ^{129}I / ^{127}I ratios in crater lake and hot spring at Zao volcano, Miyagi Prefecture

T. Matsunaka, K. Sasa, K. Sueki, N. Shibayama, T. Takahashi, M. Matsumura, Y. Satou, H. Matsuzaki[1], A. Goto[2], T. Watanabe[3], N. Tsutchiya[3], N. Hirano[3] and A. Kizaki[4]

Volcanic tremors and mountain gradient changes have been detected at Zao volcano in Miyagi since January 2013, volcanic activity has become higher after the 2011 Tohoku Earthquake although the volcano will not erupt immediately [1]. Basic water quality of crater lake and hot spring at Zao volcano have been studied by the group of Tohoku University from September 2013 since the water quality of crater lake are correlating with volcanic activity [2] [3]. As a part of this project, we are trying to monitor the volcanic activity using ^{129}I / ^{127}I ratios (atomic ratio of radioiodine and stable iodine) in crater lake and hot spring of Zao volcano. Natural ^{129}I (half-life: 15.7 million year) are produced by nuclear spallation reaction of ^{129}Xe with cosmic ray in the atmosphere and spontaneous fission of ^{238}U in the geological layer. In the ocean, steady-state ^{129}I / ^{127}I ratio of the seawater is estimated to be 1.5×10^{-12} [4]. Sunken iodine by the ocean plate having lower ^{129}I / ^{127}I ratio (older ^{129}I age) compared to the steady-state ratio of seawater, are supplied to the atmosphere mainly via magmatic activity. In general, ^{129}I / ^{127}I ratio in hot spring water and brine water are used as indicator of origin and behavior of iodine in the groundwater [5] [6]. ^{129}I / ^{127}I ratio of hydrothermal at Zao volcano are considered to become lower by the supply of chronologically-old iodine in terms of global iodine cycle.

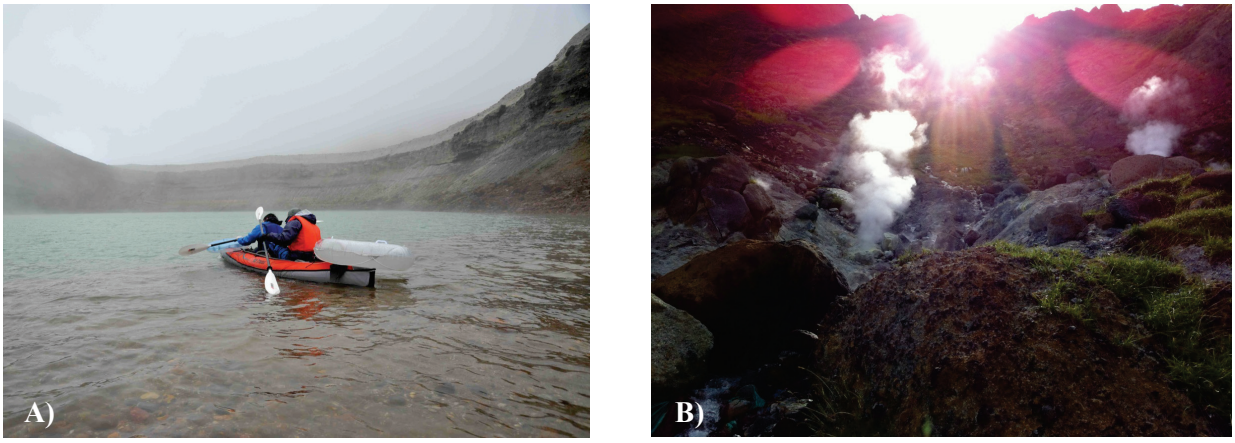

Fig.1. Photographs of sampling sites; A: Okama (crater lake), B: Kamoshika Hot Spring.

In September 2013, water samples of 2 L were collected from the surface of crater lake (Okama, diameter: 350 m, maximum depth: 35 m) located at 1,560 m in elevation and hot spring (Kamoshika Hot Spring) located at 1,230 m in elevation in the eastern side of Zao volcano (Fig.1). Water temperature and pH were measured on site. After water samples were filtered by 0.2 μm filter, ^{129}I / ^{127}I ratio were measured by AMS for the isotopic diluted water samples adding carrier (^{127}I standard) at MALT, The

[1] MALT, The University of Tokyo
[2] Center for Northeast Asian Studies, Tohoku University
[3] Graduate school of Environmental Studies, Tohoku University
[4] Faculty of Engineering and Resource Science, Akita University

University of Tokyo. ^{127}I concentrations were measured by ICP-MS, and original ^{129}I / ^{127}I ratio of water samples were estimated (Fig.2).

Water temperature and pH were 10.2℃ and 3.3 at Okama; 40.0℃ and 3.3 – 4.0 at Kamoshika Hot Spring. ^{129}I / ^{127}I ratios of Okama and Kamoshika Hot Spring were respectively, estimated to be $(1.5 \pm 0.4) \times 10^{-9}$ and $(0.78 \pm 0.15) \times 10^{-9}$, 500 – 1,000 times higher than the steady-state ratio of sea water (1.5×10^{-12}) [4]. Since ^{129}I / ^{127}I ratio of anthropogenic metric water were over 9.0×10^{-12} [7], surface water of Okama and Kamoshika Hot Spring water were very likely to be strong affected by the meteoric water including anthropogenic ^{129}I. For the monitoring of volcanic activity using ^{129}I / ^{127}I ratio, it is necessary to decide the site as few anthropogenic ^{129}I as possible through the measuring of ^{129}I / ^{127}I ratio of the Okama bottom water and some hot spring around Zao volcano. Continuous water quality survey of 1 time for Okama and 1 time per 2 months for hot springs are planned for this year.

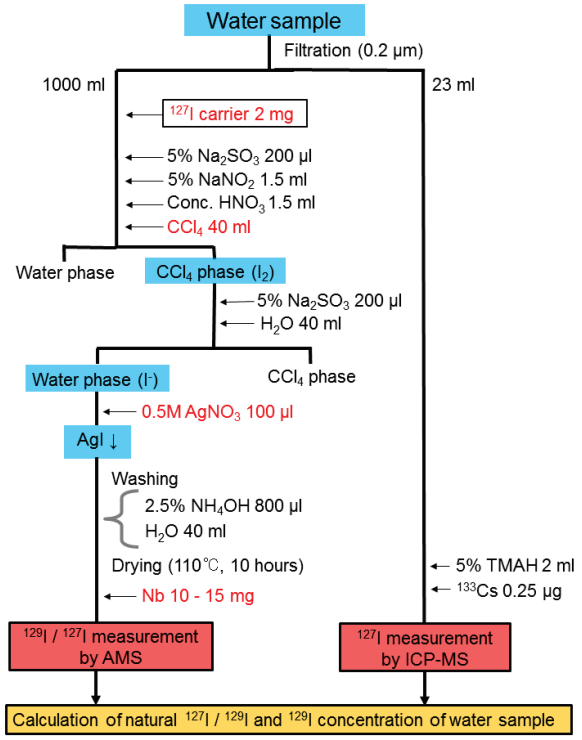

Fig.2. Sample preparation of water for the determinations of stable iodine (^{127}I) by ICP-MS and ^{129}I / ^{127}I rations by AMS.

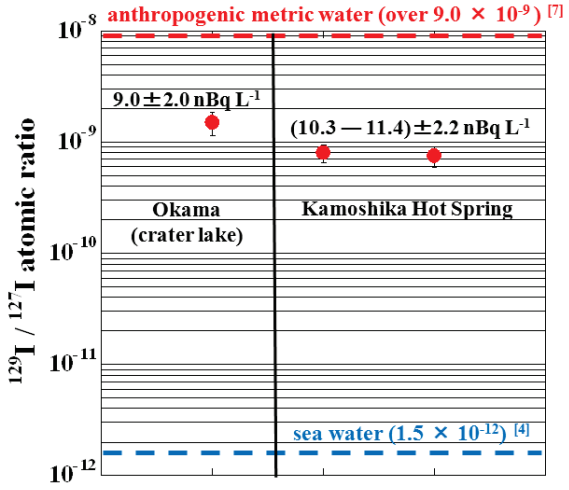

Fig.3. ^{129}I / ^{127}I ratios of Okama (crater lake) and Kamoshika Hot Spring at September 2013; red dashed line: ^{129}I / ^{127}I ratio of anthropogenic metric water, blue dashed line: ^{129}I / ^{127}I ratio of sea water.

References

[1] Japan Meteorological Agency, (2013) Monthly Volcanic Activity Report.

[2] Ohba et al., (2000) Journal of Volcanology and Geothermal Research, 97, 329-346.

[3] Ohba et al., (2008) Journal of Volcanology and Geothermal Research, 178, 131-144.

[4] Moran et al., (1998) Chemical Geology, 152, 193-203.

[5] Snyder and Fehn, (2002) Geochimica et Cosmochimica Acta, 66, 3827-3838.

[6] Muramatsu et al., (2001) Earth and Planetary Science Letter, 192, 583-593.

[7] Tomaru et al., (2007) Applied Geochemisty, 22, 676-691.

4.3 Successive searches of ^{129}I contamination in the chemical sample preparation room

M. Matsumura, K. Sasa, K. Sueki, N. Shibayama, T. Matsunaka, T. Takahashi, Y. Satou and H. Matsuzaki[1]

We have addressed measurements of trace radionuclides such as ^{36}Cl and ^{129}I by AMS. It is important that the sample preparation room must be kept clean for accurate measurement. “Clean” means that it is far from not only visible state but also invisible contamination including isobars of interests. The contamination induces confusion in experimental results for AMS. However, the sample preparation room tends to be gradually contaminated in the process of chemical treating with a high concentration of radionuclides. Especially, halogen family of elements have volatile species, and contaminant diffusion occurs in the sample preparation room easily. In this work, we show the extent of contamination in the sample preparation rooms over time, particularly pertaining to ^{129}I.

Alkaline trap solutions were placed in the several sample preparation rooms with each three weeks, at University of Tsukuba Tandem Accelerator Complex (UTTAC) and Center for Research in Isotopes and Environmental Dynamics (CRiED). After the iodine carrier was added to the part of trap solutions, the trapped iodine was collected as AgI via chemical purification. Concentrations of ^{129}I in the trap solutions were measured with the AMS at MALT, the University of Tokyo [1]. In three month intervals, the ^{129}I concentrations in the trap solutions were determined to be 10^3 to 10^4 atoms g^{-1} in the room where soil samples from Fukushima have been treated at UTTAC. On the other hand, we get results of ^{129}I concentrations in trap solutions lower than 10^3 atoms g^{-1} in the room where we have only treated samples for final purification at UTTCA, too. Besides, we find the results of highly ^{129}I contamination ranging from 10^5 to 10^6 atoms g^{-1} in the room where we treated the neutron-activated iodine at CRiED. The experimental results showed that levels of the ^{129}I contaminations depend on ambient environmental conditions in the sample preparation room (Table 1. and Fig. 1).

[1] MALT, The University of Tokyo

Table 1. Measurement of $^{129}I/^{127}I$ ratio in different rooms by AMS

Room No.	MT date	$^{129}I/^{127}I$ ($\times10^{-12}$)			^{129}I (atom g^{-1})			$^{129}I/^{127}I$ ($\times10^{-9}$)		
C108	2013/8/11	1.3	±	0.0	1.9×10^{4}	±	0.1×10^{4}	39	±	5
	2013/11/3	0.78	±	0.13	6.1×10^{3}	±	3.6×10^{3}	7.2	±	4.8
C209	2013/8/11	0.59	±	0.024	1.9×10^{3}	±	1×10^{3}	N.D.		
	2013/11/3	0.36	±	0.03	N.D.			N.D.		
CRiED cold room	2013/8/11	3.0	±	0.1	6.2×10^{4}	±	0.2×10^{4}	4.7×10^{2}	±	2.4×10^{2}
	2013/11/3	4.96	±	0.52	1.1×10^{5}	±	0.1×10^{4}	1.4×10^{2}	±	0.3×10^{2}
C210	2013/11/3	0.84	±	0.06	7.0×10^{3}	±	1.7×10^{3}	3.3	±	0.8
CRiED hot room	2013/11/3	62	±	2	1.5×10^{6}	±	0.05×10^{6}	1.2	±	0.2

Note: $^{129}I/^{127}I$ ratios were normalized by Purdue STD (63.6×10^{-12}) in the measurement. The amount of carrier was 2 mg.
The carrier solution was produced by Orion ionplus® (Thermo Fisher Scientific, USA). The $^{129}I/^{127}I$ ratios of this carrier reported were around 1.7×10^{-12} [2].

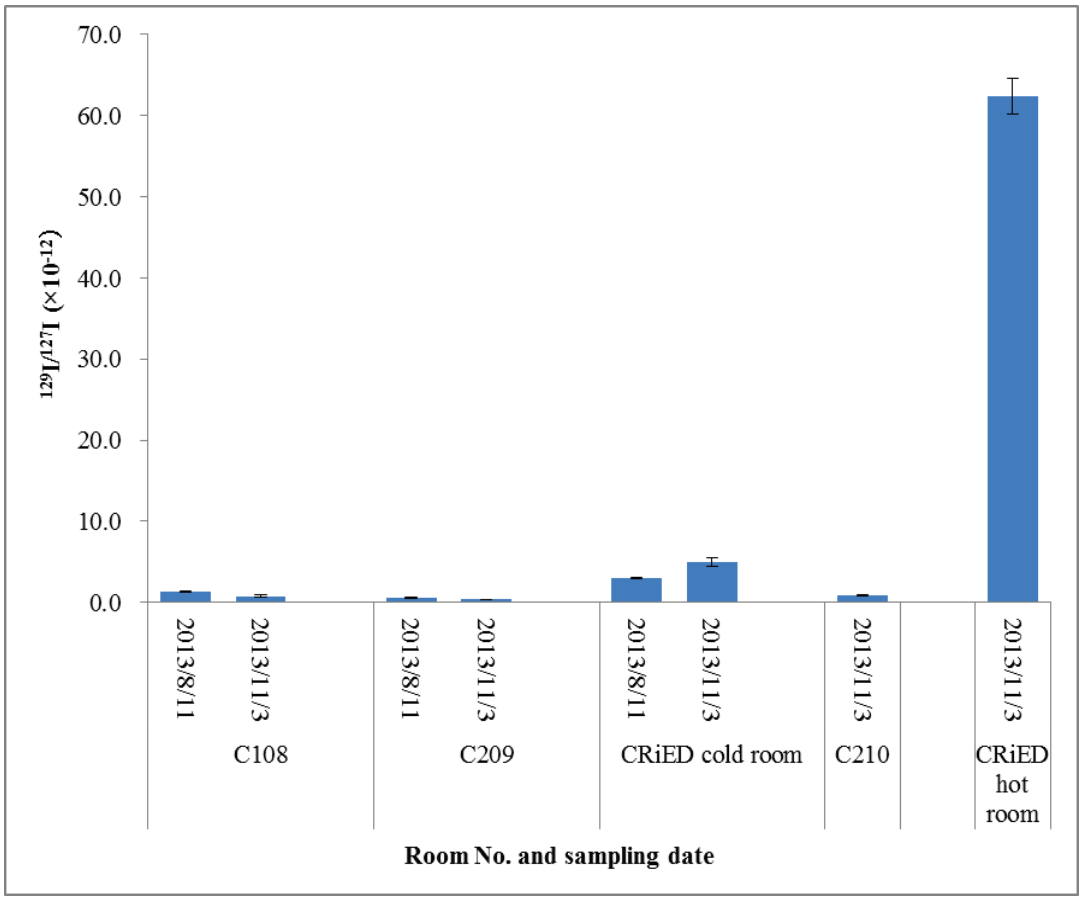

Fig.1. Comparison of $^{129}I/^{127}I$ ratios of the different rooms.

References

[1] Matsuzaki, H. et al., Nucl. Instr. and Meth. B 259 (2007) 721.

[2] Muramatsu, Y. et al., Quat.Geochro. 3(2008) 291.

4.4 Comparison between ^{36}Cl-AMS simulations using PHITS code and experiments

D. Izumi, K. Sasa, T. Takahashi, T. Matsunaka, Y. Satou, M. Matsumura, K. Sueki, M. Kinoshita[1], Y. Miyake[2] and H. Matsuzaki[2]

Update of the tandem accelerator is planned in the University of Tsukuba Tandem Accelerator Complex (UTTAC). Our group had worked on applied studies using ^{36}Cl-AMS with an old accelerator system. The maximum terminal voltage will fall down from 12 MV to 6 MV due to the update. We have investigated a material of window and gas pressure of a gas ionization detector because separation of isobars depends on energy of projectile and these detector condition. As the first step of that purpose, we simulated energy spectrum and the energy loss of ^{36}Cl in the detector using PHITS code (Particle and Heavy Ion Transport code System) [1] and results of the simulation were compared with those performed at MALT, the University of Tokyo. As shown in experimental results (Fig. 1), ^{36}Cl couldn't be separated completely from ^{36}S on two-dimensional spectrum.

Ions of $^{36}Cl^{7+}$ with 40 MeV were measured with the gas ionization detector which was filled with 60 Torr P10 gas (Ar 90% +CH_4 10%). A 3 μm of Mylar foil was used in the detector window. We obtained two-dimensional energy spectra of ^{36}Cl and ^{36}S. On the other hand, the spectra were compared with simulations using PHITS code. As a spectrum is seen in Fig. 2, the simulation showed that tail of ^{36}S interfered detection of ^{36}Cl. The tail would be caused by multiple scattering in the Mylar foil. To avoid multiple scattering, If a 150-nm-thick-silicon nitride foil (Si_3N_4) is used in the detector window, the scattering would be avoided because of its small energy loss [2]. As a spectrum is seen in Fig. 3, these results and more analysis of detector condition for optimization using the simulation would allow us to separate the isobars in the ^{36}Cl-AMS. As a result of simulation in Fig. 3, the silicon nitride entrance window will apply the new ^{36}Cl-AMS system at UTTAC.

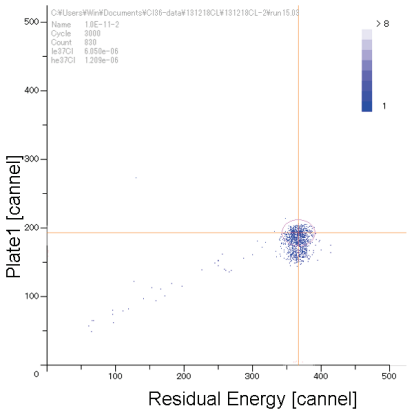

Fig.1. Two-dimensional spectrum of AMS for 40-MeV-^{36}Cl and ^{36}S performed at MALT.

[1] Institute of technology, Shimizu Co.

[2] MALT, the University of Tokyo

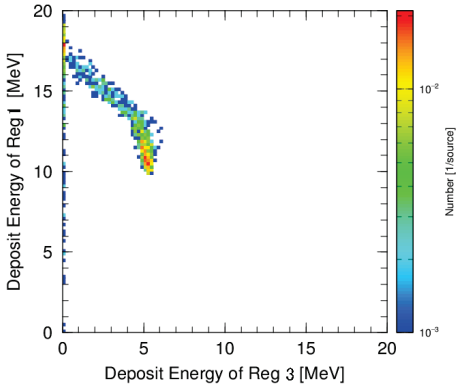

Fig.2. Two-dimensional spectrum for 40-MeV-^{36}Cl and ^{36}S with 3-μm-thick-Mylar foil simulated using PHITS code.

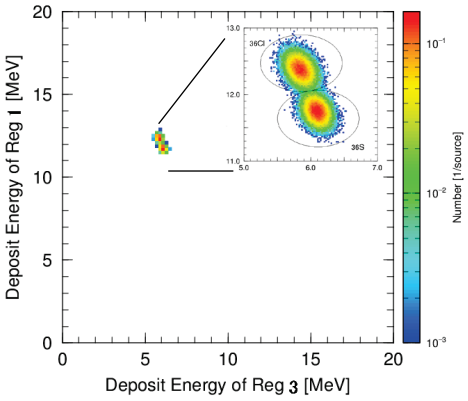

Fig.3. Two-dimensional spectrum for 40-MeV-^{36}Cl and ^{36}S with 150-nm-thick-silicom nitride foil simulated using PHITS code.

References

[1] T. Sato, K. Niita, N. Matsuda, S. Hashimoto, Y. Iwamoto, S. Noda, T. Ogawa, H. Iwase, H. Nakashima, T. Fukahori, K. Okumura, T. Kai, S. Chiba, T. Furuta and L. Sihver, Particle and Heavy Ion Transport Code System PHITS, Version 2.52, J. Nucl. Sci. Technol. 50, 913–923 (2013).

[2] C. Maden, P.A.F. Anastasi, A. Dougans, S.P.H.T. Freeman, R. Kitchen, G. Klody, C. Schnabel, M. Sundquist, K. Vanner, S. Xu, SUERC AMS ion detection, Nucl. Instr. Meth. B 259, 131–139 (2007).

4.5 Distribution of ^{129}I in the environment released from the FDNPP accident and estimation of ^{131}I/^{129}I ratio

K. Sasa, M. Matsumura, M. Matsunaka, T. Takahashi, Y. Satou, K. Sueki, N. Kinoshita[1]
and H. Matsuzaki[2]

Radioiodine is one of the most important radionuclides released from the Fukushima-Daiichi Nuclear Power Plant (FDNPP) accident. ^{131}I (half-life: 8 d) has a short half life time. We measured ^{131}I concentrations in surface soils by a gamma-ray measurement immediately after the FDNPP accident at 108 sites in Fukushima and the Kanto area [1]. Because of the difficulty of measuring ^{131}I at this time, it is expected to estimate ^{131}I precipitation from ^{129}I (half-life: 1.57×10^7 y) with the long half-life in surface soils. Therefore, it is necessary to know the isotopic ratio of ^{131}I/^{129}I released from the FDNPP accident for reconstruction of ^{131}I. ^{129}I/^{127}I ratio was measured by accelerator mass spectrometry (AMS) at MALT, the University of Tokyo [2]. Stable iodine of ^{127}I was determined by inductively coupled plasma mass spectrometry (ICP-MS). We got a result that the average of ^{129}I concentration was $(2.74 \pm 1.35) \times 10^8$ atoms/g prior to the FDNPP accident as ^{129}I background data at Fukushima. After the FDNPP accident, the weighted average of ^{131}I /^{129}I ratios is estimated to $(4.02 \pm 0.81) \times 10^{-2}$ at Fukushima as at March 11, 2011. Fig. 1 shows a correlation between ^{129}I and ^{131}I in surface soils. The calculation results of ^{131}I/^{129}I ratio made by ORIGEN 2.2 code [3] are 3.18×10^{-2} for the Unit 1, 4.57×10^{-2} for the Unit 2 and 4.81×10^{-2} for the Unit 3. They are consistent with the measured results of ^{131}I /^{129}I ratio.

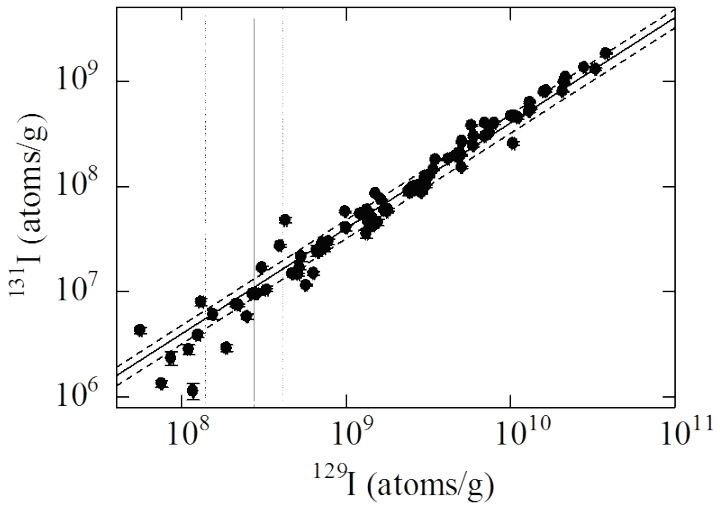

Figure 1. Correlation between ^{129}I and ^{131}I in surface soils at Fukushima as at March 11, 2011. Black line shows the weighted average of ^{131}I/^{129}I ratios. Dashed line indicates the standard deviation of 1σ.

References

[1] Norikazu Kinoshita, Keisuke Sueki, Kimikazu Sasa et al., *PNAS*, 108 (2011) 19526-19529.

[2] Hiroyuki Matsuzaki et al., *Nucl. Instr. Meth. Phys. Res.* B 259, (2007) 721-726.

[3] Kenji Nishihara, *JAEA-Data/Code* 2012-018.

[1] Shimizu Co.
[2] MALT, The University of Tokyo

4.6 Technological development for Strontium-90 determination using AMS

Y. Satou, K. Sueki, K. Sasa, T. Matsunaka, T. Takahashi, N. Shibayama, D. Izumi, N. Kinoshita[1] and H. Matsuzaki[2]

Strontium-90 (^{90}Sr) is a fission product and expected to be released into the environment through such as a nuclear accident. ^{90}Sr quantities are usually measured by chemical isolation of Sr from environmental samples followed by low-level beta counting, however, there are complicated and time-consuming processes to determine ^{90}Sr. Rapid and simple processes are highly required to evaliate ^{90}Sr quantities, especially after the nuclear disaster. The Accelerator Mass Spectrometry (AMS) is one of potential methods which would solve these problems. We have attempted to develop the ^{90}Sr-AMS using the 5 MV tandem accelerator at MALT, the University of Tokyo. We report production tests of negative ion beams and detection tests of ^{90}Zr with the AMS techniques for effective ^{90}Sr measurements. Target samples of SrF_2 were made with chemical separation from the soil at Fukushima. Mixed samples with the purified SrF_2 and PbF_2 were pressed in the aluminum sample holder and installed in the MC-SNICS ion source. The negative ions of $^{88}SrF_3^-$ with over 500 nA were successfully extracted from the MC-SNICS ion source. Natural isobar of ^{90}Zr interferes with ^{90}Sr detection using an ionization chamber. However, in order to observe the behavior of the ^{90}Sr in gas counter, ^{90}Zr isobar was monitored as ^{90}Sr in this study. After the ions passed through a gas stripper, the ions with 90 for mass number and 6+ for charge state, which are considered to be ^{90}Zr, were transported to an ionization chamber. The ions with 1000 cps for count rate were identified in the two-dimensional spectrum in Fig. 1, which correspond to approximately 3×10^{-8} for atom ratio of ^{90}Zr/^{88}Sr in the Sr beam. Further works would provide a successful isobaric separation.

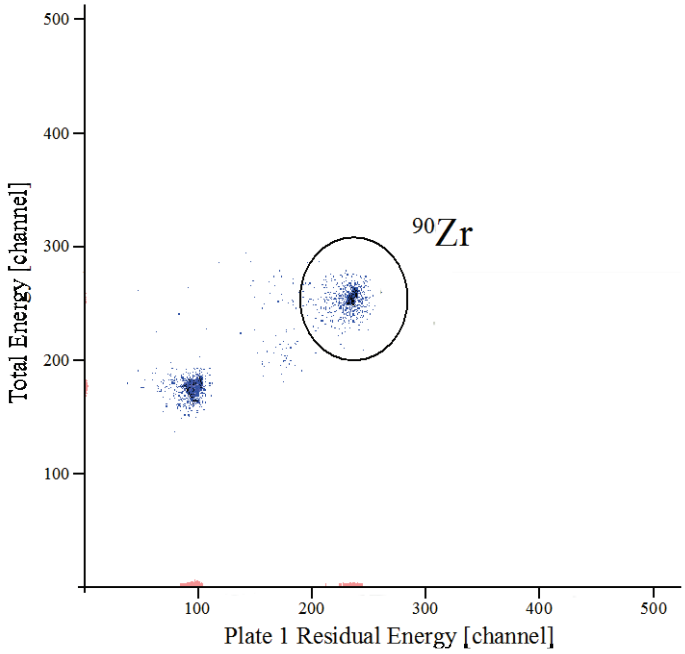

Fig.1 Spectrum of $^{90}Zr^{6+}$ on gas counter.

[1] Institute of Technology, Shimizu Corporation
[2] MALT, The University of Tokyo

5. LIST OF PUBLICATIONS

ACCELERATOR AND EXPERIMENTAL FACILITIES

1. K. Sasa, "The 6 MV tandem accelerator project for nuclear physics and ion beam applications at the University of Tsukuba", *AIP Conf. Proc.***1533**,184 (2013).

NUCLEAR PHYSICS

2. L.Y. Zhang, J.J. He, A. Parikh, S.W. Xu, H. Yamaguchi, D. Kahl, S. Kubono, P. Mohr, J. Hu, P. Ma, S.Z. Chen, Y. Wakabayashi, H.W. Wang, W.D. Tian, R.F. Chen, B. Guo, T. Hashimoto, Y. Togano, S. Hayakawa, T. Teranishi, N. Iwasa, T. Yamada, T. Komatsubara, Y.H. Zhang, X.H. Zhou, "Investigation of the thermonuclear ^{18}Ne(α, p)^{21}Ne reaction rate via resonant elastic scattering of ^{21}Na + p", *Phys. Rev. C* **89**, 015804 (2014).

3. S.J. Jin, Y.B. Wang, J. Su, S.Q. Yan, Y.J. Li, B. Guo, Z.H. Li, S. Zeng, G. Lian, X.X. Bai, W.P. Liu, H. Yamaguchi, S. Kubono, J. Hu, D. Kahl, H.S. Jung, J.Y. Moon, C.S. Lee, T. Teranishi, H.W. Wang, H. Ishiyama, N. Iwasa, T. Komatsubara, B.A. Brown, "Resonant scattering of ^{22}Na + p studied by the thick-target inverse-kinematic method", *Phys. Rev. C* **88**, 035801 (2013).

4. J.J. He, L.Y. Zhang, A. Parikh, S.W. Xu, H. Yamaguchi, D. Kahl, S. Kubono, J. Hu, P. Ma, S.Z. Chen, Y. Wakabayashi, B.H. Sun, H.W. Wang, W.D. Tian, R.F. Chen, B. Guo, T. Hashimoto, Y. Togano, S. Hayakawa, T. Teranishi, N. Iwasa, T. Yamada, T. Komatsubara, "The ^{18}Ne(α, p)^{21}Na breakout reaction in x-ray bursts: Experimental determination of spin-parities for α resonances in ^{22}Mg via resonant elastic scattering of ^{21}Na + p", *Phys. Rev. C* **88**, 012801(R) (2013).

5. C.B. Moon, T. Komatsubara, K. Furuno, "Level structure of ^{154}Ho", *Phys. Rev. C* **88**, 044308 (2013).

6. K. Setoodehnia, A.A. Chen, D. Kahl, T. Komatsubara, J. Jose, R. Longland, Y. Abe, D.N. Binh, J. Chen, S. Cherubini, J.A. Clark, C.M. Deibel, S. Fukuoka, T. Hashimoto, T. Hayakawa, J. Hendriks, Y. Ishibashi, Y. Ito, S. Kubono, W.N. Lennard, T. Moriguchi, D. Nagae, R. Nishikiori, T. Niwa, A. Ozawa, P.D. Parker, D. Seiler, T. Shizuma, H. Suzuki, C. Wrede, H. Yamaguchi, T. Yuasa, "Nuclear structure of ^{30}S and its implications for nucleosynthesis in classical novae", *Phys. Rev. C* **87**, 065801 (2013).

7. T. Onishi, T. Komatsubara, T. Yuasa, K. Sasa, A. Ozawa, D. Izumi, M. Mukai, S. Kubono, T. Hayakawa, T. Shizuma, "Study of nucleosynthesis by means of ^{45}Sc + p reaction", *JPS (The Physical*

Society of Japan) Conf. Proc. **1**, 013054 (2014).

8. T. Komatsubara, T. Yuasa, T. Onishi, Y. Saito, S. Okada, K. Sasa, A. Ozawa, T. Hayakawa, T. Shizuma, T. Kajino, S. Kubono, "Study for big bang nucleosynthesis concerning lithium isotopes", *JPS (The Physical Society of Japan) Conf. Proc.* **1**, 013055 (2014).

9. K. Setoodehnia, A. A. Chen, D. Kahl, T. Komatsubara, J. Jos, R. Longland, Y. Abe, D. N. Binh, J. Chen, S. Cherubini, J. A. Clark, C. M. Deibel, S. Fukuoka, T. Hashimoto, T. Hayakawa, J. Hendriks, Y. Ishibashi,Y. Ito, S. Kubono, W. N. Lennard, T. Moriguchi, D. Nagae, R. Nishikiori, T. Niwa, A. Ozawa, P. D . Parker, D. Seiler, T. Shizuma, H. Suzuki, C. Wrede, H. Yamaguchi, T. Yuasa, "Nuclear structure of ^{30}S and its implications for nucleosynthesis in classical novae", *Phys. Rev. C* **87**, 065801 (2013).

10. Y. Ito, P. Schury, M. Wada, S. Naimi, T. Sonoda, H. Mita, F. Arai, A. Takamine, K. Okada, A. Ozawa, H. Wollnik, "Single-reference high-precision mass measurement with a multireflection time-of-flight mass spectrograph", *Phys. Rev. C* **88**, 011306(R) (2013).

11. T. Moriguchi, A. Ozawa, S. Ishimoto, Y. Abe, M. Fukuda, I. Hachiuma, Y. Ishibashi, Y. Ito, T. Kuboki, M. Lantz, D. Nagae, K. Namihira, D. Nishimura, T. Ohtsubo, H. Ooishi, T. Suda, H. Suzuki, T. Suzuki, M. Takechi, K. Tanaka, T. Yamaguchi, "Density distributions of ^{11}Li deduced from reaction cross-section measurements", *Phys. Rev. C* **88**, 024610 (2013).

12. H.J. Ong, I. Tanihata, A. Tamii, T. Myo, K. Ogata, M. Fukuda, K. Hirota, K. Ikeda, D. Ishikawa, T. Kawabata, H. Matsubara, K. Matsuta, M. Mihara, T. Naito, D. Nishimura, Y. Ogawa, H. Okamura, A. Ozawa, D. Y. Pang, H. Sakaguchi, K. Sekiguchi, T. Suzuki, M. Taniguchi, M. Takashina, H. Toki, Y. Yasuda, M. Yosoi, J. Zenihiro, "Probing effect of tensor interactions in ^{16}O via (p,d) reaction", *Phys. Let. B* **725**,277 (2013).

13. T. Yamaguchi, Y. Yamaguchi, A. Ozawa, "The challenge of precision mass measurements of short-lived exotic nuclei, "Development of a new storage ring mass spectrometry", *Int. J. of Mass Spectrometry* **349–350**, 240 (2013).

14. Yu.A. Litvinov, S. Bishop, K. Blaum, F. Bosch, C. Brandau, L.X. Chen, I. Dillmann, P. Egelhof, H. Geissel, R.E. Grisenti, S. Hagmann, M. Heil, A. Heinz, N. Kalantar-Nayestanaki, R. Knoobel, C. Kozhuharov, M. Lestinsky, X.W. Ma, T. Nilsson, F. Nolden, A. Ozawa, R. Raabe, M.W. Reed, R. Reifarth, M.S. Sanjari, D. Schneider, H. Simon, M. Steck, T. Stoohlker, B.H. Sun, X.L. Tu, T. Uesaka, P.M. Walker, M. Wakasugi, H. Weick, N. Winckler, P.J. Woods, H.S. Xu, T. Yamaguchi, Y. Yamaguchi, Y.H. Zhang, "Nuclear physics experiments with ion storage rings", *Nucl. Instrum. Meth. Phys. Res. B* **317**, 603 (2013).

15. Y. Yamaguchi, M. Wakasugi, T. Uesaka, A. Ozawa, Y. Abe, T. Fujinawa, M. Kase, M. Komiyama, T. Kubo, K. Kumagai, T. Maie, D. Nagae, J. Ohnishi, F. Suzaki, A. Tokuchi, Y. Watanabe, K. Yoshida, K. Yamada, T. Yamaguchi, H. Yamasawa, Y. Yanagisawa, J. Zenihiro, Y. Yano, "Construction of rare-RI ring at RIKEN RI Beam Factory", *Nucl. Instrum. Meth. Phys. Res. B* **317**, 629 (2013).

16. F. Suzaki, J. Zenihiro, T. Yamaguchi, A. Ozawa, T. Uesaka, M. Wakasugi, K. Yamada, Y. Yamaguchi, Rare-RI Ring collaboration, "Design study of a resonant Schottky pick-up for the Rare-RI Ring project", *Nucl. Instrum. Meth. Phys. Res. B* **317**, 636 (2013).

17. D. Nagae, Y. Abe, S. Okada, A. Ozawa, T. Yamaguchi, H. Suzuki, T. Moriguchi, Y. Ishibashi, S. Fukuoka, R. Nishikiori, T. Niwa, T. Suzuki, F. Suzaki, K. Sato, H. Furuki, N. Ichihashi, S. Miyazawa, Y. Yamaguchi, T. Uesaka, M. Wakasugi, "Time-of-flight detector applied to mass measurements in Rare-RI Ring", *Nucl. Instrum. Meth. Phys. Res. B* **317**, 640 (2013).

18. T. Yamaguchi, F. Suzaki, T. Izumikawa, S. Miyazawa, K. Morimoto, T. Suzuki, F. Tokanai, H. Furuki, N. Ichihashi, C. Ichikawa, A. Kitagawa, T. Kuboki, S. Momota, D. Nagae, M. Nagashima, Y. Nakamura, R. Nishikiori, T. Niwa, T. Ohtsubo, A. Ozawa, K. Sato, S. Sato, S. Suzuki, "Performance of high-resolution position-sensitive detectors developed for storage-ring decay experiments", *Nucl. Instrum. Meth. Phys. Res. B* **317**, 697 (2013).

19. S. Yamaki, T. Yamaguchi, J. Kouno, K. Sato, N. Ichihashi, T. Suzuki, K. Abe, Y. Abe, M. Fukuda, H. Furuki, N. Inaba, K. Iwamoto, T. Izumikawa, Y. Kamisho, N. Kikuchi, A. Kitagawa, M. Mihara, S. Miyazawa, S. Momota, Y. Morita, D. Nagae, M. Nagashima, Y. Nakamura, R. Nishikiori, D. Nishimura, I. Nishizuka, T. Ohtsubo, J. Ohno, A. Ozawa, T. Sakai, S. Sato, D. Sera, F. Suzaki, S. Suzuki, S. Suzuki, M. Wakabayashi, M. Yaguchi, S. Yasumoto, "Systematic study of individual charge-changing cross sections of intermediate-energy secondary beams", *Nucl. Instrum. Meth. Phys. Res. B* **317**, 774 (2013).

20. Y. Ishibashi, N. Yoshida, H. Ueno, A. Yoshimi, Y. Ichikawa, Y. Abe, K. Asahi, M. Chikamori, T. Fujita, T. Furukawa, E. Hikota, D. Nagae, Y. Ohtomo, Y. Saito, H. Shirai, T. Suzuki, X.F. Yang, N. Sakamoto, "Development of an adiabatic field rotation system to measure spin polarization of unstable nuclei", *Nucl. Instrum. Meth. Phys. Res. B* **317**, 714 (2013).

21. Y. Ishibashi, D. Nagae, Y. Abe, T. Nagatomo, A. Ozawa, H. Suzuki, S. Fukuoka, R. Nishikiori, T. Niwa, K. Matsuta, Y. Tagishi, "Production of nuclear polarization of unstable nuclei via polarization transfer reactions", *Hyperfine Interact.* **220**, 71 (2013).

22. N. Yoshida, H. Ueno, A. Yoshimi, Y. Ishibashi, Y. Ichikawa, Y. Abe, K. Asahi, M. Chikamori, T. Fujita, T. Furukawa, E. Hikota, D. Nagae, Y. Ohtomo, Y. Saito, H. Shirai, T. Suzuki, X.F. Yang, "Development of a new device control system for β-NMR experiments", *Nucl. Instrum. Meth. Phys. Res. B* **317**, 705 (2013).

23. X.F. Yang, T. Furukawa, T. Wakui, K. Imamura, H. Tetsuka, T. Fujita, Y. Yamaguchi, Y. Tsutsui, Y. Mitsuya, Y. Ichikawa, Y. Ishibashi, N. Yoshida, H. Shirai, Y. Ebara, M. Hayasaka, S. Arai, S. Muramoto, A. Hatakeyama, M. Wada, T. Sonoda, Y. Ito, T. Kobayashi, S. Nishimura, M. Nishimura, Y. Kondo, K. Yoneda, H. Ueno, T. Shinozuka, T. Shimoda, K. Asahi, Y. Matsuo, "Control of stopping position of radioactive ion beam in superfluid helium for laser spectroscopy experiments", *Nucl. Instrum. Meth. Phys. Res. B* **317**, 599 (2013).

24. D. Nagae, T. Niwa, Y. Ishibashi, Y. Abe, S. Fukuoka, R. Nishikiori, S. Okada, Y. Saito, N. Inaba, A. Ozawa, Y. Aoki, "Development of rotating magnetic field system for the β-NMR method", The 4th Joint Meeting of the International Symposium on Hyperfine Interactions and the International Symposium on Nuclear Quadrupole Interactions (HFI/NQI 2012) *Hyperfine Interact.* **220**, 65-69 (2013).

25. M. Mihara, K. Matsuta, D. Nishimura, M. Fukuda, M. Yaguchi, K. Iwamoto, M. Wakabayashi, Y. Kamisho, J. Ohno,Y. Morita, T. Izumikawa, T. Ohtsubo, S. Suzuki, M. Nagashima, K. Abe, T. Sakai, S. Momota, A. Ozawa, D. Nagae,Y. Ishibashi, Y. Abe, T. Niwa, T. Nagatomo, T. Minamisono, M. K. Kubo, A. Kitagawa, M. Torikoshi, M. Kanazawa , S. Sato, "Production of spin polarized 12N through heavy ion reactions", The 4th Joint Meeting of the International Symposium on Hyperfine Interactions and the International Symposium on Nuclear Quadrupole Interactions (HFI/NQI 2012) *Hyperfine Interact.* **220**, 83 (2013).

26. Y. Yamaguchi , M. Wakasugi, T. Uesaka, A. Ozawa, Y. Abe, T. Fujinawa, M. Kase, M. Komiyama, T. Kubo, K. Kumagai, T. Maie, D. Nagae, J. Ohnishi, F. Suzaki, A. Tokuchi, Y. Watanabe, K. Yoshida, K. Yamada, T. Yamaguchi, H. Yamasawa, Y. Yanagisawa, J. Zenihiro, Y. Yano, "Construction of rare-RI ring at RIKEN RI Beam Factory", *Proceedings of the XVIth International Conference on Electromagnetic Isotope Separators and Techniques Related to their Applications, Nucl. Instrum. Meth. Phys. Res. B* **317**, 629 (2013).

27. D. Nagae, Y. Abe, S. Okada, A. Ozawa, T. Yamaguchi, H. Suzuki, T. Moriguchi, Y. Ishibashi, S. Fukuoka, R. Nishikiori, T. Niwa, T. Suzuki, F. Suzaki, K. Sato, H. Furuki, N. Ichihashi, S. Miyazawa, Y. Yamaguchi, T. Uesaka, M. Wakasugi, "Time-of-flight detector applied to mass measurements in Rare-RI Ring", *Proceedings of the XVIth International Conference on Electromagnetic Isotope Separators and Techniques Related to their Applications, Nucl. Instrum. Meth. Phys. Res. B* **317**, 640 (2013).

28. T. Yamaguchi, F. Suzaki, T. Izumikawa, S. Miyazawa, K. Morimoto, T. Suzuki, F. Tokanai, H. Furuki, N. Ichihashi, C. Ichikawa, A. Kitagawa, T. Kuboki, S. Momota, D. Nagae, M. Nagashima, Y. Nakamura, R. Nishikiori, T. Niwa, T. Ohtsubo, A. Ozawa, K. Sato, S. Sato, S. Suzuki, "Performance of high-resolution position-sensitive detectors developed for storage-ring decay experiments", *Proceedings of the XVIth International Conference on Electromagnetic Isotope Separators and Techniques Related to their Applications, Nucl. Instrum. Meth. Phys. Res. B* **317**, 697 (2013).

29. N. Yoshida, H. Ueno, A. Yoshimi, Y. Ishibashi, Y. Ichikawa, Y. Abe, K. Asahi, M. Chikamori, T. Fujita, T. Furukawa, E. Hikota, D. Nagae, Y. Ohtomo, Y. Saito, H. Shirai, T. Suzuki, X.F. Yang, "Development of a new device control system for β-NMR experiments", *Proceedings of the XVIth International Conference on Electromagnetic Isotope Separators and Techniques Related to their Applications, Nucl. Instrum. Meth. Phys. Res. B* **317***,* 705 (2013).

30. Y. Ishibashi, N. Yoshida, H. Ueno, A. Yoshimi, Y. Ichikawa, Y. Abea, K. Asahi, M. Chikamori, T. Fujita, T. Furukawa, E. Hikota, D. Nagae, Y. Ohtomo, Y. Saito, H. Shirai, T. Suzuki, X.F. Yang, N. Sakamoto, "Development of an adiabatic field rotation system to measure spin polarization of 315unstable nuclei", *Proceedings of the XVIth International Conference on Electromagnetic Isotope Separators and Techniques Related to their Applications, Nucl. Instrum. Meth. Phys. Res. B* **317**, 714 (2013).

31. S. Yamaki, T. Yamaguchi, J. Kouno, K. Sato, N. Ichihashi, T. Suzuki, K. Abe, Y. Abe, M. Fukuda, H. Furuki, N. Inaba, K. Iwamoto, T. Izumikawa, Y. Kamisho, N. Kikuchi, A. Kitagawa, M. Mihara, S. Miyazawa, S. Momota, Y. Morita, D. Nagae, M. Nagashima, Y. Nakamura, R. Nishikiori, D. Nishimura, I. Nishizuka, T. Ohtsubo, J. Ohno, A. Ozawa, T. Sakai, S. Sato, D. Sera, F. Suzaki, S. Suzuki, S. Suzuki, M. Wakabayashi, M. Yaguchi, S. Yasumoto, "Systematic study of individual charge-changing cross sections of intermediate-energy secondary beams", *Proceedings of the XVIth International Conference on Electromagnetic Isotope Separators and Techniques Related to their Applications, Nucl. Instrum. Meth. Phys. Res. B* **317**, 774 (2013).

32. A.S. Demyanova, A.A. Ogloblin, A.N. Danilov, S.V. Dmitriev, S.A. Goncharov, N. Burtebaev, J. Burtebaeva,N. Saduev, T.L. Belyaeva, H. Suzuki, A. Ozawa, Y. Abe, S. Fukuoka, Y. Ishibashi, S. Ito, T. Komatsubara,T. Moriguchi, D. Nagae, R. Nishikiori, T. Niwa, K. Okumura, H. Ooishi, K. Yokoyama and S. Kubono, "Spectroscopy of ^{9}Be and observation of neutron halo structure in the states of positive parity rotational band", *Proceedings of International Nuclear Physics Conference, EPJ Web of Conferences* **66**, 02026 (2014).

33. M. Takechi, S. Suzuki, D. Nishimura, M. Fukuda, T. Ohtsubo, M. Nagashima, T. Suzuki, T. Yamaguchi,A. Ozawa, T. Moriguchi, H. Ohishi, T. Sumikama, H. Geissel, M. Ishihara, N. Aoi,

Rui-Jiu Chen,De-Qing Fang, N. Fukuda, S. Fukuoka, H. Furuki, N. Inabe, Y. Ishibashi, T. Itoh, T. Izumikawa, D. Kameda, T. Kubo, C. S. Lee, M. Lantz, Yu-Gang Ma, K. Matsuta, M. Mihara, S. Momota, D. Nagae, R. Nishikiori,T. Niwa, T. Ohnishi, K. Okumura, T. Ogura, H. Sakurai, K. Sato, Y. Shimbara, H. Suzuki, H. Takeda,S. Takeuchi, K. Tanaka, H. Uenishi, M. Winkler, Y. Yanagisawa, S. Watanabe, K. Minomo, S. Tagami,M. Shimada, M. Kimura, T. Matsumoto, Y. R. Shimizu and M. Yahiro, "Search for halo nucleus in Mg isotopes through the measurements of reaction cross sections towards the vicinity of neutron drip line", *Proceedings of International Nuclear Physics Conference, EPJ Web of Conferences* **66**, 02101 (2014).

34. S. Suzuki, M. Takechi, T. Ohtsubo, D. Nishimura, M. Fukuda, T. Kuboki, M. Nagashima, T. Suzuki, T. Yamaguchi, A. Ozawa, H. Ohishi, T. Moriguchi, T. Sumikama, H. Geissel, N. Aoi, Rui-Jiu Chen,De-Qing Fang, N. Fukuda, S. Fukuoka, H. Furuki, N. Inabe, Y. Ishibashi, T. Ito, T. Izumikawa, D. Kameda,T. Kubo, M. Lantz, C.S. Lee, Yu-Gang Ma, M. Mihara, S. Momota, D. Nagae, R. Nishikiori, T. Niwa,T. Ohnishi, K. Okumura, T. Ogura, H. Sakurai, K. Sato, Y. Shimbara, H. Suzuki, H. Takeda, S. Takeuchi,K. Tanaka, H. Uenishi, M. Winkler and Y. Yanagisawa, "Measurements of interaction cross sections for $^{22-35}$Na isotopes", *Proceedings of International Nuclear Physics Conference, EPJ Web of Conferences* **66**, 03084 (2014).

35. M. von Schmid, S. Bagchi, S. Bönig, M. Csatlós, I. Dillmann, C. Dimopoulou, P. Egelhof, V. Eremin,T. Furuno, H. Geissel, R. Gernhäuser, M. N. Harakeh, A.-L. Hartig, S. Ilieva, N. Kalantar-Nayestanaki,O. Kiselev, H. Kollmus, C. Kozhuharov, A. Krasznahorkay, T. Kröll, M. Kuilman, S. Litvinov,Yu. A. Litvinov, M. Mahjour-Shafiei, M. Mutterer, D. Nagae, M. A. Najafi, C. Nociforo, F. Nolden, U. Popp,C. Rigollet, S. Roy, C. Scheidenberger, M. Steck, B. Streicher, L. Stuhl, M. Thürauf, T. Uesaka, H. Weick,J. S. Winfield, D. Winters, P. J. Woods, T. Yamaguchi, K. Yue, J. C. Zamora and J. Zenihiro, "First EXL experiment with stored radioactive beam: Proton scattering on ^{56}Ni", *Proceedings of International Nuclear Physics Conference, EPJ Web of Conferences* **66**, 03093 (2014).

36. S. Yamaki, J. Kouno, D. Nishimura, M. Nagashima, M. Takechi, K. Sato, K. Abe, Y. Abe, M. Fukuda,H. Furuki, I. Hachiuma, A. Homma, N. Ichihashi, C. Ichikawa, N. Inaba, T. Ito, K. Iwamoto, T. Izumikawa,Y. Kamisho, N. Kikuchi, S. Kinno, A. Kitagawa, T. Kojima, T. Kuboki, M. Mihara, S. Miyazawa, S. Momota, Y. Morita, D. Nagae, Y. Nakamura, K. Namihira, R. Nishikiori, I. Nishizuka, T. Niwa, M. Ogura, Y. Ohkuma, T. Ohtsubo, S. Okada, J. Ohno, A. Ozawa, Y. Saito, T. Sakai, S. Sato, D. Sera, F. Suzaki, S. Suzuki, S. Suzuki, T. Suzuki, M. Taguchi, H. Uenishi, M. Wakabayashi, D. Watanabe, M. Yaguchi, S. Yasumoto andT. Yamaguchi, "Charge-changing interactions probing point-proton radii of nuclei", *Proceedings of International Nuclear Physics Conference, EPJ Web of Conferences* **66**, 03099 (2014).

37. Y. Abe, D. Nagae, the Rare-RI Ring collaboration,"Developments of time-of-flight detectors for Rare-RI Ring", *JPS Conf. Proc.* **1**, 013059 (2014).

38. H. Tsuchida, T. Majima, S. Tomita, K. Sasa, K. Narumi, Y. Saitoh, A. Chiba, K. Yamada, K. Hirata, H. Shibata, A. Itoh, "Transmission properties of C_{60} ions through micro- and nano-capillaries", *Nucl. Instrum. Meth. Phys. Res. B* **315**, 336 (2013).

39. A. Suzuki, Y. Hirose, D. Oka, S. Nakao, T. Fukumura, S. Ishii, K. Sasa, H. Matsuzaki, T. Hasegawa, "High-Mobility Electron Conduction in Oxynitride: Anatase TaON", *Chem. Mater.* **26**, 976(2014).

40. T. Onishi, T. Komatsubara, T. Yuasa, K. Sasa, A, Ozawa, D. Izumi, M. Mukai, S. Kubono, T. Hayakawa and T. Shizuma, "Study of Nucleosynthesis By Means of ^{45}Sc + p Reaction", *Proceedings of the 12th Asia Pacific Physics Conference, JPS Conf. Proc.* 013054 (2014).

41. T. Komatsubara, T. Yuasa, T. Onishi, Y. Saito, S. Okada, K., Sasa, A. Ozawa, T. Hayakawa, T. Shizuma, T. Kajino, S. Kubono, "Study for Big Bang Nucleosynthesis Concerning Lithium Isotopes", *Proceedings of the 12th Asia Pacific Physics Conference, JPS Conf. Proc.* 013055 (2014).

42. E. Kita, K.Z. Suzuki, Y. Liu, Y. Utsumi, J. Morishita, D. Oshima, T. Kato, T. Niizeki, K. Mibu, H. Yanagihara, "Magnetization control for bit pattern formation of spinel ferromagnetic oxides by Kr ion implantation" , *J. Appl. Phys.* **115,** 17B907(2014).

43. E. Kita, K. Ono, N. Yamaguchi, T. Nishihashi, M. Iura, J. Morishita, Y. Utsumi, T. Murakami, K. Mibu, T. Niizeki, K.Z. Suzuki, H. Yanagihara, "Magnetization control in spinel-type Fe_3O_4 thin films by ion implantation", *Jpn. J. Appl. Phys.* **53** 020306(2014).

44. M. Kishimoto, K. Asai, D. Isaka, H. Yanagihara, Y. Nagasaki, E. Kita, "Magnetic properties in oriented platelet Fe_3O_4 particles prepared by the polyol method using α-FeOOH as precursors", *J. Magn. Magn. Mater.* **352,** 13 (2014).

45. A. Sagara, M. Hiraiwa, A. Uedono, N. Oshima, R. Suzuki, S. Shibata, "Residual defects in low-dose arsenic-implanted silicon after high-temperature annealing", *Nucl. Instrum. Meth. Phys. Res. B* **321**, 54 (2014).

46. A. Uedono, S. Murakami, K. Inagaki, K. Iseki, N. Oshima, R. Suzuki, "Characterization of polyethylene terephthalate films coated with thin $Al_xSi_{1-x}O_y$ layers using monoenergetic positron beams", *Thin Solid Films* **552**, 82 (2013).

47. S. Sellaiyan, A. E. Hughes, S. V. Smith, A. Uedono, J. Sullivan, S. Buckman, “Leaching properties of chromate-containing epoxy films using radiotracers, PALS and SEM”, *Prog. Organic Coat.* **77**, 257 (2014).

48. H. Shimizu, S. Nagano, A. Uedono, N. Tajima, T. Momose, Y. Shimogaki, “Material design of plasma-enhanced chemical vapour deposition SiCH films for low-k cap layers in the further scaling of ultra-large-scale integrated devices-Cu interconnects”, *Sci. Tech. Adv. Mat.* **44**, 055005 (2013).

49. A. Uedono, T. Watanabe, S. Kimura, Y. Zhang, M. Lozac’h, L. Sang, S. Ishibashi, N. Oshima, R. Suzuki, M. Sumiya, “Vacancy-type defects in $In_xGa_{1-x}N$ grown on GaN templates probed using monoenergetic positron beams”, *J. Appl. Phys.* **114**, 184504 (2013).

50. A. Uedono, P. Verdonck, A. Delabie, J. Swerts, T. Witters, T. Conard, M. R. Baklanov, S. Van Elshocht, N. Oshima, R. Suzuki, “Characterization of Porous Structures in Advanced Low-k Films with Thin TaN Layers Using Monoenergetic Positron Beams”, *Jpn. Appl. Phys.* **52**, 106501 (2013).

51. A. Uedono, I. Yonenaga, T. Watanabe, S. Kimura, N. Oshima, R. Suzuki, S. Ishibashi, Y. Ohno, “Vacancy-type defects introduced by plastic deformation of GaN studied using monoenergetic positron beams”, *J. Appl. Phys.* **114**, 084506 (2013).

52. A. Uedono, T. Kirimura, C. J. Wilson, K. Croes, S. Demuynck, Z. Tőkei, N. Oshima, R. Suzuki, “Vacancy reactions near the interface between electroplated Cu and barrier metal layers studied by monoenergetic positron beams”, *J. Appl. Phys.* **114**, 074510 (2013).

53. P. Verdonck, A. Maheshwari, J. Swerts, A. Delabie, T. Witters, H. Tielens, S. Dewilde, A. Franquet, J. Meersschaut, T. Conard, J. L. Prado, S. Armini, M. R Baklanov, S. Van Elshocht, A. Uedono, D. R. Huanca, S. G. dos Santos, G. Kellerman, “The Effects of Plasma Treatments and Subsequent Atomic Layer Deposition on the Pore Structure of a k=2.0 Low-k Material”, *ECS J. Solid State Sci. Tech.* **2** N103 (2013).

54. S. F. Chichibu, T. Onuma, K. Hazu, A. Uedono, “Time-resolved luminescence studies on AlN and high AlN mole fraction AlGaN alloys”, *Phys. Stat. Sol. C* **10**, 501 (2013).

55. S. F. Chichibu, H. Miyake, Y. Ishikawa, M. Tashiro, T. Ohtomo, K. Furusawa, K. Hazu, K. Hiramatsu, A. Uedono, “Impacts of Si-doping and resultant cation vacancy formation on the luminescence dynamics for the near-band-edge emission of $Al_{0.6}Ga_{0.4}N$ films grown on AlN templates by metalorganic vapor phase epitaxy”, *J. Appl. Phys.* **113**, 213506 (2013).

56. A. Uedono, S. Ishibashi, N. Oshima, R. Suzuki, “Positron annihilation spectroscopy on nitride-based

semiconductors", *Jpn. J. Appl. Phys.* **52**, 08JJ02 (2013).

57. A. Uedono, T. Tsutsui, T. Watanabe, S. Kimura, Y. Zhang, M. Lozac'h, L. W. Sang, S. Ishibashi, M. Sumiya, "Point defects introduced by InN alloying into $In_xGa_{1-x}N$ probed using a monoenergetic positron beam", *J. Appl. Phys.* **113**, 123502 (2013).

58. M. Jiang, D. D. Wang, Z. Q. Chen, S. Kimura, Y. Yamashita, A. Mori, A. Uedono, "Chemical effect of Si^+ ions on the implantation-induced defects in ZnO studied by a slow positron beam", *J. Appl. Phys.* **113**, 043506 (2013).

59. M. M. Islam, A. Uedono, T. Sakurai, A. Yamada, S. Ishizuka, K. Matsubara, S. Niki, K. Akimoto, "Impact of Se flux on the defect formation in polycrystalline Cu(In,Ga)Se_2 thin films grown by three stage evaporation process", *J. Appl. Phys.* **113**, 064907 (2013).

MATERIALS AND CLUSTER SCIENCE

60. K. Ozeki, D. Sekiba, K.K. Hrakuri, T. Masuzawa, "Antithrombogenicity of Amorphous deuterated carbon film prepared by RF-plasma CVD", *Nano Biomedinine* **5**,11 (2013).

6. THESES

Master's theses

Momo MUKAI	Search for efficient laser resonance ionization schemes of refractory elements for KISS
Kazuki OSHIMA	Long-range angular correlation including forward rapidity detector in LHC-ALICE p-Pb collisions at $\sqrt{s_{NN}}$=5.02TeV
Hitomi OZAKI	Measurements of η dependence of higher harmonic flow for charged hadron in $\sqrt{s_{NN}}$=200GeV Cu+Au collisions at RHIC-PHENIX
Yuta SAITO	Charge radius of ^{33}Cl deduced from the charge changing cross section
Takahiro ONISHI	Study of ^{45}Sc(p,α)^{42}Ca reaction in low energy region
Taiyo KOBAYASHI	Study on associated low pT hadron production with di-jet in Pb-Pb collisions at $\sqrt{s_{NN}}$=2.76 TeV in LHC-ALICE
Shunsuke OKADA	Developments of Time-of-fright detector in Rare RI Ring
Koichi KIHARA	System size dependence of higher harmonic azimuthal anisotropy for charged hadrons via two-particle correlations at RHIC-PHENIX
Naoto TANAKA	Azimuthally sensitive HBT in $\sqrt{s_{NN}}$ =2.76TeV Pb-Pb collisions at LHC-ALICE
Naruki INABA	Measurement of the sign of instability jittery magnetic moment by β-NMR with rotating magnetic field
Kenta CHITO	Development of high-resolution ERDA and resolution estimation by a-C:H film
Isao HARAYAMA	Development of ΔE-E telescope ERDA for absolute quantification of metal nitro-oxide nano thin films
Yoko SHIINA	Coincidence measurements of secondary electrons and transmitted ions under irradiation of fast cluster ions

Undergraduate theses

Satomi MAEDA	Detection system development of backscattered particle for channeling experiments
Yoshihiko YATSU	Development of experimental setup for the zero degree electron spectroscopy under fast cluster irradiation on carbon thin foils
Ryousuke WATANABE	Coincidence measurements of secondary electrons and transmitted ions under irradiation of fast cluster ions through solid materials

7. SEMINARS

2013

Jul 25 High-precision mass measurement of short-lived nuclei with a multi-reflection time-of-flight mass spectrograph, *Yuta Ito (University of Tsukuba)*

Aug 8 Nuclear structure and space nucleosynthesis, *Tetsuro Komatsubara (University of Tsukuba)*

2014

Jan 20 Search for efficient laser resonance ionization schemes of refractory elements for KISS, *Momo Mukai (University of Tsukuba)*

Long-range angular correlation including forward rapidity detector in LHC-ALICE p-Pb collisions at $\sqrt{s_{NN}}$=5.02TeV, *Kazuki Oshima (University of Tsukuba)*

Measurements of η dependence of higher harmonic flow for charged hadron in $\sqrt{s_{NN}}$=200GeV Cu+Au collisions at RHIC-PHENIX, *Hitomi Ozaki (University of Tsukuba*

Charge radius of ^{33}Cl deduced from the charge changing cross section, *Yuta Saito (University of Tsukuba)*

Jan 21 Study of ^{45}Sc(p,α)^{42}Ca reaction in low energy region, *Takahiro Onishi (University of Tsukuba)*

Study on associated low pT hadron production with di-jet in Pb-Pb collisions at $\sqrt{s_{NN}}$=2.76 TeV in LHC-ALICE, *Taiyo Kobayashi (University of Tsukuba)*

Developments of Time-of-fright detector in Rare RI Ring, *Shunsuke Okada (University of Tsukuba)*

Jan 23 System size dependence of higher harmonic azimuthal anisotropy for charged hadrons via two-particle correlations at RHIC-PHENIX, *Koichi Kihara (University of Tsukuba)*

Azimuthally sensitive HBT in $\sqrt{s_{NN}}$=2.76TeV Pb-Pb collisions at LHC-ALICE, *Naoto Tanaka (University of Tsukuba)*

Measurement of the sign of instability jittery magnetic moment by β-NMR with rotating magnetic field, *Naruki Inaba (University of Tsukuba)*

8. SYMPOSIUM

A research prospect of multi-tandem accelerator facility at University of Tsukuba – Innovation and development of new aspect by means of 6 MV tandem accelerator

18 March 2014

Laboratory of Advanced Research B 0110

1. Openning : *E. Kita (University of Tsukuba)*

2. Future prospects of nuclear physics experiments by 6 MV tandem accelerator at University of Tsukuba : *A. Ozawa (University of Tsukuba)*

3. SIMS of amino-acids by swift C60+ ion transmission : *K. Nakajima (University of Kyoto)*

4. PIXE analyses of trace elements in fluid inclusions from a granite and meteorites : *M. Kurosawa (University of Tsukuba)*

5. Towards understanding the mechanism of cluster effects on the secondary electron yield : *S. Tomita (University of Tsukuba)*

6. Limit of detection and application of high-resolution ERDA : *D. Sekiba (University of Tsukuba)*

7. Development of high sensitive palmtop sensor with etched tracks : *K. Awazu (National Institute of Advanced Industrial Science and Technology (AIST))*

8. Future prospects of ion beam applications by 6 MV tandem accelerator at University of Tsukuba : *K. Sasa (University of Tsukuba)*

9. Closing remarks : *D. Sekiba (University of Tsukuba)*

9. LIST OF PERSONNEL

Tandem Accelerator Complex

E. Kita	Director, Professor
K. Sasa	Associate Professor
D. Sekiba	Assistant Professor
H. Kimura	Computer Engineer
H. Oshima	Electrical Engineer
Y. Tajima	Mechanical Engineer
S. Ishii	Mechanical Engineer
T. Takahashi	Electrical Engineer
Y. Yamato	Electrical Engineer
S. Selvakumar	Research Fellow
M. Matsumura	Research Supporter
K. Miya	Administrative Staff
M. Ohyama	Administrative Staff
Y. Matsuda	Administrative Staff
N. Yamada	Administrative Staff
H. Muromachi	Administrative Staff

Research Members[1]

Inst. of Physics

I. Arai	T. Matsunaka	D. Nagae	A.Ozawa
K. Sasa			

Inst. of Applied Physics

K. Akimoto	S. Aoki	E. Kita	M. Minagawa
D. Sekiba	T. Suemasu	S. Tomita	A. Uedono
H. Yanagihara	Y. Watahiki		

Inst. of Materials Science

T. Kondo	M. Takahashi

[1]The "research members" include the authors and coauthors within 5 years back from this fiscal year, as well as the members of research projects running at UTTAC.

Inst. of Geoscience

M. Kurosawa

Inst. of Chemistry

K. Sueki

Staff of Open Advanced Facilities Initiative

H. Kudo	H. Naramoto	H. Muromachi

Graduate students

Doctoral Programs of Pure and Applied Science

Y. Abe	S. Fukuoka	Y. Ishibashi	K. Ito
K. Kurita	S. Kimura		

Master's Programs of Pure and Applied Science

R. Aoyama	F. Arai	K. Chito	I. Harayama
A. Horiuchi	N. Inaba	D. Izumi	Y. Liu
S. Kimura	R. Kinoshita	A. Mori	J. Morishita
M. Mukai	S. Okada	T. Onishi	Y. Saito
T. Sanai	Y. Satou	K. Sawahata	Y. Shiina
Y. Utsumi	T. Watanabe	K. Yamazaki	Z. Yang
Y. Yasutomi	N. Yoshihara		

Undergraduates

H. Alime	A. Kamezawa	S. Maeda	T. Oguro
T. Senba	K. Watanabe	R. Watanabe	Y. Yatsu

Scientific Gutests and Fellows

K. Awazu	National Institute of Advanced Industrial Science and Technology (AIST)
M. Fujimaki	National Institute of Advanced Industrial Science and Technology (AIST)
Y. Tosaki	National Institute of Advanced Industrial Science and Technology (AIST)

T. Hayakawa	Japan Atomic Energy Agency (JAEA)
T. Shizuma	Japan Atomic Energy Agency (JAEA)
S. Kubono	Center for Nuclear Study, the Univ. of Tokyo (CNS)
A. Sato	Osaka Univ.
A. Yamamoto	High Energy Accelerator Research Organization (KEK)
T. Adachi	High Energy Accelerator Research Organization (KEK)
M. Yoshida	High Energy Accelerator Research Organization (KEK)
N. Kawamura	High Energy Accelerator Research Organization (KEK)
K. Shimomura	High Energy Accelerator Research Organization (KEK)
P. Strasser	High Energy Accelerator Research Organization (KEK)
T. Nakamoto	High Energy Accelerator Research Organization (KEK)
M. Iio	High Energy Accelerator Research Organization (KEK)
K. Yoshimura	High Energy Accelerator Research Organization (KEK)